UNIVERSITAT POLITÈCNICA DE CATALUNYA
BARCELONATECH
Facultat d'Òptica i Optometria de Terrassa

MÀSTER UNIVERSITARI EN OPTOMETRIA I CIÈNCIES DE LA VISIÓ

TREBALL FINAL DE MÀSTER

"Study of air flow and temperature on corneal Surface using a model eye"

Elisabet Simó Bertran

Director: Genís Cardona Torradeflot
Tutors: Paul Murphy i Melanie Mungalsingh
Departament: Òptica i Optometria

Terrassa, 22 de Gener de 2020
Facultat d'Òptica i Optometria de Terrassa

UNIVERSITAT POLITÈCNICA DE CATALUNYA
BARCELONATECH
Facultat d'Òptica i Optometria de Terrassa

Elisabet Simó Bertran

MÀSTER UNIVERSITARI EN OPTOMETRIA I CIÈNCIES DE LA VISIÓ

"Study of air flow and temperature on corneal Surface using a model eye"

RESUM

L'estesiòmetre d'aire és un instrument no invasiu que s'està desenvolupant per a millorar la tècnica de mesura de la sensibilitat corneal. L'objectiu d'aquesta investigació, la qual forma part d'un projecte més gran en el marc d'una tesi doctoral a la Universitat de Waterloo (Canada), era participar en el desenvolupament i avaluació d'un nou estesiòmetre estudiant les característiques del seu flux d'aire i els canvis de temperatura que aquest produeix. Primer, es va analitzar la força de l'aire que sortia del estesiòmetre mitjançant una microbalança. Les lectures de la balança (g) augmenten segons la intensitat de sortida d'aire de l'aparell. Després, es va estudiar la dispersió del flux d'aire que emet l'estesiòmetre mitjançant pols de licopodi. El diàmetre dels craters generats per la dispersió de la pols són més grans quan la intensitat de l'aparell augmenta i els resultats de la ploma de pols corresponent també es veuen alterats. Finalment, es mesurava la mida en diàmetre de la petjada tèrmica generada per l'aire, utilitzant la càmera tèrmica FLIR A655sc (FLIR Systems Inc., Portland, USA) i un ull model desenvolupat a la mateixa Universitat de Waterloo per l'equip de "Murphy Laboratory for Experimental Optometry (MLEO)". En aquest cas, la petjada tèrmica és més gran a mesura que augmenta la distància entre l'estesiòmetre i l'ull model. A més, per intensitats baixes el diàmetre és més petit que per a intensitats altes. Com a conclusió, és necessària més recerca per determinar les característiques òptimes de l'estímul per les mesures *in vivo.* De moment, sembla que hi hagi relació entre la mida del diàmetre trobat al segon experiment i la petjada tèrmica del tercer experiment. També s'ha trobat en els tres experiments una relació on la durada de l'estímul no és un factor tant crític com la intensitat de la sortida d'aire de l'aparell, que es podria considerar el paràmetre més rellevant. La termografia també es mostra com una modalitat d'imatge fiable per estudiar els canvis de temperatura de la superfície corneal.

Paraules clau: estesiòmetre, còrnia, sensibilitat corneal, termografia.

UNIVERSITAT POLITÈCNICA DE CATALUNYA
BARCELONATECH
Facultat d'Òptica i Optometria de Terrassa

Elisabet Simó Bertran

MÀSTER UNIVERSITARI EN OPTOMETRIA I CIÈNCIES DE LA VISIÓ

"Study of air flow and temperature on corneal Surface using a model eye"

RESUMEN

El estesiómetro de aire es un instrumento no invasivo que se está desarrollando para mejorar la técnica de medida de la sensibilidad corneal. El objetivo de esta investigación, que forma parte de un proyecto más amplio, en el marco de una tesis doctoral en la Universidad de Waterloo (Canada), era participar en el desarrollo y evaluación de un nuevo estesiómetro estudiando los parámetros de su flujo de aire y los cambios de temperatura que este produce. Primero, se analizó la fuerza ejercida por el aire que emitía el estesiómetro a partir de una microbalanza. Las lecturas de la balanza (g) augmentan según la intensidad del flujo de aire del aparato. Después, se estudió la dispersión del flujo de aire que salía del estesiómetro mediante polvo de licopodio. El diámetro de los cráteres generados por la dispersión del polvo es más grande cuando la intensidad del aire augmenta y los resultados de la pluma de polvo correspondiente también se ven alterados. Finalmente, se media el tamaño de la huella térmica generada por el aire, utilizando la camera térmica FLIR A655sc (FLIR Systems Inc., Portland, USA) y un ojo modelo desarrollado en la misma Universidad de Waterloo por el equipo de "Murphy Laboratory for Experimental Optometry (MLEO)". En este caso, la huella térmica es mayor a medida que augmenta la distancia entre el estesiómetro y el ojo modelo. Además, para intensidades bajas el diámetro es más pequeño que para intensidades altas. Como conclusión, se necesita más investigación para determinar las características óptimas del estímulo para las medidas *in vivo*. De momento, parece ser que hay una relación entre la medida del diámetro encontrado en el segundo experimento y la huella térmica del tercero. También se ha encontrado en los tres experimentos una relación donde el tiempo del estímulo no es un factor tan crítico como la intensidad de salida de aire del estesiómetro, que se podría considerar el parámetro más relevante. La termografía también demostró ser una modalidad de imagen fiable para estudiar los cambios de temperatura de la superficie corneal.

Palabras clave: estesiometría, cornea, sensibilidad corneal, termografía.

UNIVERSITAT POLITÈCNICA DE CATALUNYA
BARCELONATECH
Facultat d'Òptica i Optometria de Terrassa

Elisabet Simó Bertran

MÀSTER UNIVERSITARI EN OPTOMETRIA I CIÈNCIES DE LA VISIÓ

Study of air flow and temperature on corneal Surface using a model eye

ABSTRACT

The non-contact corneal aesthesiometer (NCCA) is a non-invasive instrument being developed to measure corneal sensitivity. The objective of this research, which is part of a larger project leading to a PhD thesis at the University of Waterloo (Canada), was to assist in the development and evaluation of a new NCCA by studying the air-flow parameters and the temperature changes using a model eye. First, the force exerted by the exit-jet was analyzed using a microbalance. Microbalance readings (g) increased with the intensity of the air-flow. Second, the dispersion of the air-flow exiting the aesthesiometer was studied using lycopodium powder. The diameters of the craters resulting from dispersion of the powder were larger at higher intensities and the corresponding dust plume was also altered. Finally, the thermal footprint size of the air-flow was measured using the FLIR A655sc infrared camera (FLIR Systems Inc., Portland, USA) and a model eye developed by the Murphy Laboratory for Experimental Optometry (MLEO). In this case, for longer distances between the aesthesiometer and the model eye the results of the footprint showed larger diameters. In addition, at low intensities of the air-jet the footprint size was smaller. More research is needed to determine the best characteristics of the stimulus for *in vivo* measurements but a good relationship was found between the diameter of the crater in the experiment with lycopodium powder and the thermal footprint size. The three experiments were in agreement in that the duration of the stimulus was not as critical a factor as the intensity of the air-jet, which could be considered the most relevant parameter. Thermography was also shown as a valuable imaging modality to study ocular surface temperature changes.

Keywords: aesthesiometer, cornea, corneal sensibility, thermography.

ACKNOWLEDGEMENTS

To Genis, Paul and Melanie who gave me the chance
and my family and friends who provided their support and unconditional love.

This project is written in an article format aiming to be sent to *Contact Lens Anterior Eye* (Elsevier). This magazine belongs to the British Contact Lens Association and occupies the place 29/59 (Q2) in the Ophthalmology category of the Journal Citation Reports, with an Impact Factor of 1.985 (2018).

Instructions for the authors of the magazine can be found in Annex 4.

Elisabet Simó Bertran

Study of air flow and temperature on corneal Surface using a model eye

E. Simó Bertran[1], G. Cardona Torradeflot[1], P. Murphy[2], M. Mungalsingh[2]

[1]Facultat d'Òptica i Optometria, Tr8 Building, Violinista Vellsolà St 37, Technical University of Catalonia, 08222 Terrassa, Barcelona, Spain.

[2] School of Optometry and Vision Science, Columbia St W, University of Waterloo, N2L3G1 Waterloo, Ontario, Canada.

ABSTRACT

The non-contact corneal aesthesiometer (NCCA) is a non-invasive instrument being developed to measure corneal sensitivity. The objective of this research, which is part of a larger project leading to a PhD thesis at the University of Waterloo (Canada), was to assist in the development and evaluation of a new NCCA by studying the air-flow parameters and the temperature changes using a model eye. First, the force exerted by the exit-jet was analyzed using a microbalance. Microbalance readings (g) increased with the intensity of the air-flow. Second, the dispersion of the air-flow exiting the aesthesiometer was studied using lycopodium powder. The diameters of the craters resulting from dispersion of the powder were larger at higher intensities and the corresponding dust plume was also altered. Finally, the thermal footprint size of the air-flow was measured using the FLIR A655sc infrared camera (FLIR Systems Inc., Portland, USA) and a model eye developed by the Murphy Laboratory for Experimental Optometry (MLEO). In this case, for longer distances between the aesthesiometer and the model eye the results of the footprint showed larger diameters. In addition, at low intensities of the air-jet the footprint size was smaller. More research is needed to determine the best characteristics of the stimulus for in vivo measurements but a good relationship was found between the diameter of the crater in the experiment with lycopodium powder and the thermal footprint size. The three experiments were in agreement in that the duration of the stimulus was not as critical a factor as the intensity of the air-jet, which could be considered the most relevant parameter. Thermography was also shown as a valuable imaging modality to study ocular surface temperature changes.

Keywords: aesthesiometer, cornea, corneal sensibility, thermography.

Elisabet Simó Bertran

1. Introduction

The cornea is considered to be one of the most innervated tissues of the human body. Corneal innervation plays a role in protecting the tissue from adverse factors that can be detrimental to its integrity and metabolism [1,2,3,4]. Any alteration in the sensitivity of the cornea may compromise the functional unit of the tear, thus leading to the development of dry eye disease, as well as impacting the ability to detect any foreign body that could cause significant damage to the ocular surface [5]. A regular control of corneal sensitivity is important to aid in the prevention and management of ocular surface alterations such as dry eye, keratitis, and herpes, and to assess the decreased corneal sensitivity often associated with eye surgeries, diabetes, and the use of contact lenses and therapeutic agents [6].

The cornea is innervated by the ophthalmic division of the trigeminal nerve, through the long ciliary nerves. Corneal innervation contributes to maintaining the integrity of the ocular surface through fostering cell growth and the proliferation of epithelial cells, wound healing, and repair [7,8]. Stimuli to the cornea are detected by free nerve endings, which consist of two types of axons: the first type is the myelinated A-delta fibers, which respond to mechanical stimuli, and conduct nerve impulses quickly; the second type of nerve fibers are the C-fibers, which respond to thermal, mechanical, and chemical stimuli. Unlike the A-delta fibers, the C-fibers are unmyelinated, which results in a slower conduction rate of nerve impulses. The C-fibers represent the majority of the sensory nerves reaching the cornea, and act as a polymodal nociceptors [9,10].

Corneal sensitivity is measured using an instrument known as an aesthesiometer. Sensitivity is the inverse of the threshold response to a stimulus, which can be mechanical, chemical, or thermal. Von Frey started stimulating the corneal nerves mechanically using horse hairs in 1894. This method was later modified first by Boberg-Ans in 1955, and then by Cochet-Bonnet. The Cochet-Bonnet aesthesiometer (COBO) is known as the gold standard aesthesiometer and involves stimulating the mechanosensory nerve fibers (specifically the A-delta fibers) pressing the cornea with a nylon thread. However, this method is not only very invasive, but may also be affected by many external agents, such as room temperature and humidity, maintenance of the device, technique and expertise of the examiner, and patient apprehension [1,11,12,13] These limitations have led to the development of other aesthesiometers which allow the measurement of corneal sensitivity to mechanical, chemical, or thermal stimuli, whilst avoiding contact with the ocular surface [14].

One such example is the non-contact corneal aesthesiometer (NCCA) engineered by Murphy and associates [11]. This non-invasive instrument uses a controlled mechanical pulse of air to stimulate the cornea. As the air makes contact with the cornea, a cooling effect is produced by the localized evaporation of tear film from the ocular surface, thus stimulating the thermal receptors. However, one key limitation of the device is that there is a delay of approximately 0.2 seconds in reaching maximum stimulus intensity [15]. Other non-invasive aesthesiometers developed over the years have added other stimuli such as temperature (hot and cold air pulses), and chemical substances (irritant chemical stimuli) to assess corneal sensitivity [14,16,17]. However, with these aesthesiometers there is often an overlapping of stimuli, thus making it difficult to isolate the mechanical and thermal responses, for example [15]. To overcome the limitations of the existing aesthesiometers, the Murphy Laboratory of Experimental Optometry (MLEO) at the University of Waterloo has developed a new and improved non-invasive aesthesiometer. With new instruments it is important to understand the mechanics and the stimulus characteristics, as well as to determine the optimal parameters for testing corneal sensitivity, such as the appropriate nozzle diameter, test distance, duration, and intensity [11].

The aim of this research, which is part of a larger project leading to a PhD thesis at the University of Waterloo (Canada), was to perform several experiments to determine the optimal stimulus parameters of the air-jet of the future new aesthesiometer. The present article will describe the design and initial results of several studies, which aimed at determining: (a) the force exerted by the jet using an analytical microbalance; (b) the pattern of the air-flow using lycopodium powder and; (c) the footprint size of the air-flow stimulus using a model eye and a thermal camera.

2. Material and methods

The different combinations of the parameters used in this study were based on the results of previous work by Murphy and their co-workers [11,13,15]. A brass nozzle adapted on the exit-jet of the blower [Fig. 1] was used with the new device in order to improve performance. The exit-jet of the microblower has a diameter of 0.75 mm, which is reduced to 0.50 mm with the addition of the brass nozzle. The units used for the intensity of this new aesthesiometer are still not properly normalized, so for the moment measurements shall be labelled as "unit".

Fig. 1. Blower of the new aesthesiometer without the brass nozzle (left), brass nozzle and adaptor (centre) and brass nozzle adapted on the micro-blower (right).

2.1. Force exerted by the jet analysed with a microbalance

The force exerted by the new air jet was measured with an analytical microbalance. The micro-blower device was held in parallel to the microbalance with a metallic rod of 30 cm with a modified support capable of housing the aesthesiometer device. The rod was held horizontally with a metallic clamp and a support bar [Fig. 2]. This allowed for easy fine-tuning of the different distances required for the analysis.

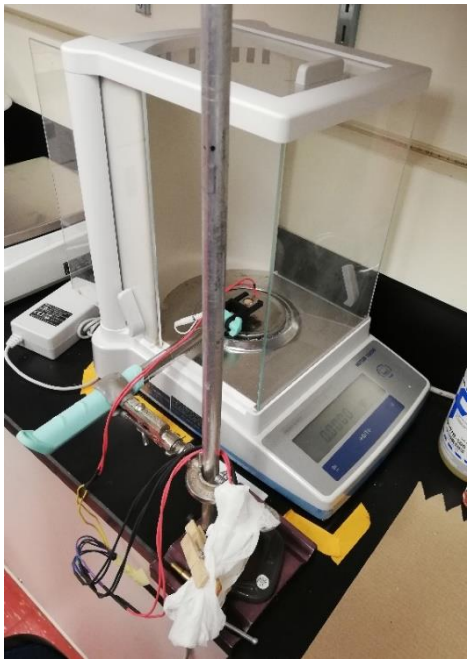

Fig. 2. Set up of microbalance and aesthesiometer.

The microbalance was calibrated before starting the experiment using a range of standard weighs from 1 mg to 100 g.

The experiment was carried out at four different distances between the microbalance and the air jet: 0.5 cm, 1 cm, 1.5 cm and 3 cm. The air pressure intensities were selected by the control unit of the air-flow and set at four different values: 250 unit, 210 unit, 140 unit and 70 unit. In addition, five different durations of air-flow were tested: 10 s, 5 s, 1.5 s, 1 s and 0.5 s. For each combination of these parameters, ten consecutive measurements were conducted to determine the repeatability of the procedure. Results were recorded as grams.

2.2. Pattern of the air-flow

The study of the dispersion of the air-flow exiting the aesthesiometer was first performed by Boberg-Ans (1952), and repeated by Murphy (1996) to further the understanding of these phenomena. The aim of this part of the study was to repeat those experiments with the new prototype of aesthesiometer.

A rectangular (28 x 14.7 cm) paper frame was used as a limiting surface over which a thin layer of lycopodium powder was spread. An adaptable support was employed to hold the air jet parallel to the surface, with the nozzle directed to the powder. This set up permitted placing the micro-blower exit-jet at four different distances from the surface with powder: 0.5 cm, 1 cm, 1.5 cm and 3 cm. The aesthesiometer control unit was adjusted for a continuous air-flow at room temperature of 22˚C and three different durations: 0.5 s, 0.9 s and 1.5 s. The stimulus intensity of the air-flow was set at four different values: 250 unit, 210 unit, 140 unit and 70 unit. These parameters were selected according to published literature for the evaluation of air exit volume and the determination of the resulting diameters [5,11,15].

Each measurement was repeated two times for each predetermined distance so eight craters were registered on the powder surface. A ruler was attached next to the rectangular card as a reference measure to determine the diameter of the craters during posterior image analysis with the freely available software ImageJ v.151 (National Institutes of Health, US) [Fig. 3]. Measurements were conducted without and with the brass nozzle attached to the aesthesiometer.

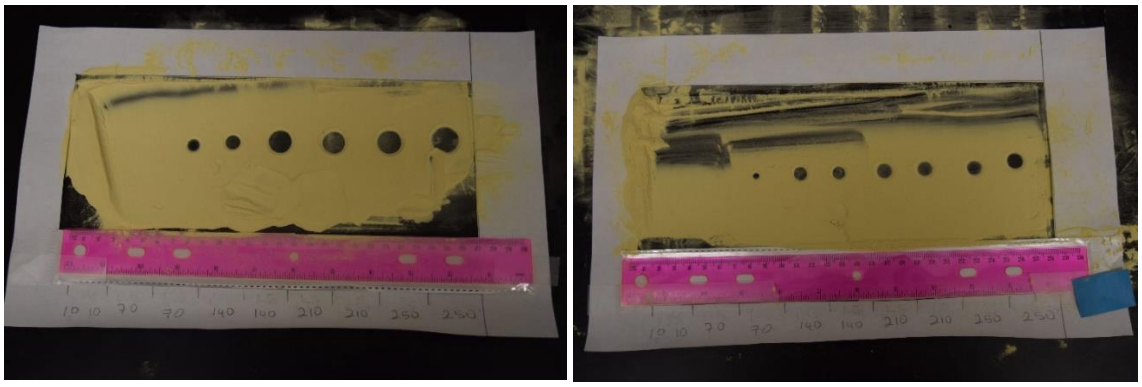

Fig. 3. Trial at 1.0 cm distance and with an air-flow duration of 0.9 s without (left) and with (right) the brass nozzle adapted on the exit-jet.

A similar set up was used to visualize the air-flow laterally. The rectangular limiting base was covered with a plastic surface with a small hole in the middle. In this case, the micro-blower was placed under the plastic base with the exit-jet pointing upwards and emerging from the hole. That protected the micro-blower from the lycopodium powder spread above.

A ruler was held perpendicular to the basis using a metallic clamp and a black cardboard was employed as background to obtain a better view of the dust plume generated by the air-flow [Fig. 4]. The aesthesiometer control unit was adjusted for a continuous flow of air of two different durations: 1 s and 10 s. Four different stimulus intensities of the air-flow were investigated: 250 unit, 210 unit, 140 unit and 70 unit.

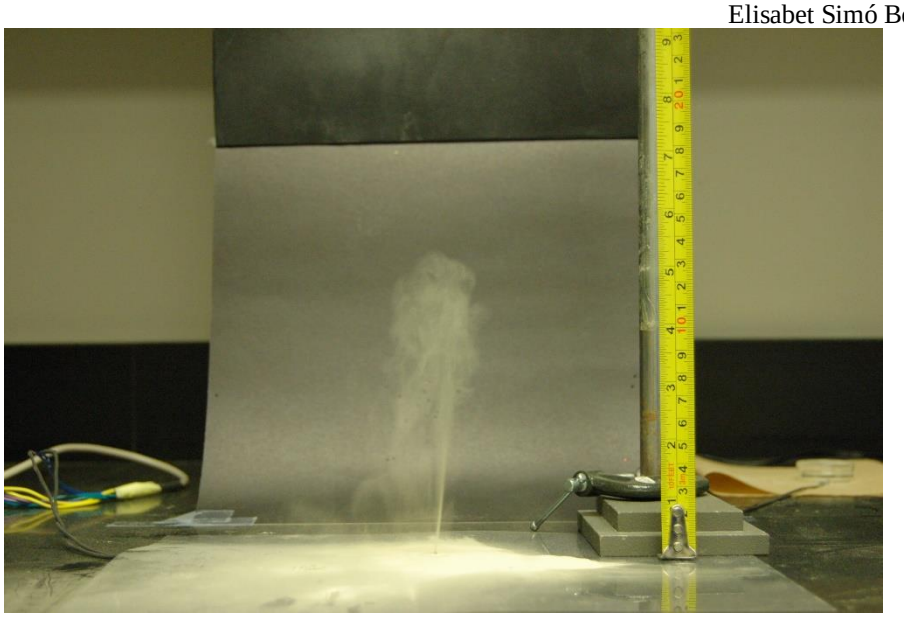

Fig. 4. Dust plume resulting from an intensity of 250 unit and air-flow duration of 10 s.

The measurements were repeated five times with all the possible combinations of the parameters. Video recordings were obtained for each measurement, and posterior frame-by-frame analysis was conducted to determine the height of the dust plume.

2.3. Footprint size of the air-flow stimulus examined with a model eye and a thermal camera

The thermal footprint size of the airflow stimulus generated by the new aesthesiometer was measured on a model eye using the FLIR A655sc infrared camera (FLIR Systems Inc., Portland, USA). The model eye design was developed by the Murphy Laboratory for Experimental Optometry (MLEO). Prior to any measurement, and to ensure similitude with the human ocular surface, the model eye was warmed at 32˚C during 45 minutes. The model eye was placed in front of the thermal camera using a metallic clamp and a vertical holder simulating the corneal surface of a real eye [Fig. 5].

The camera employed the FLIR ResearchIR Max Version 4.30.1.70 software, which permits viewing, capturing and recording for posterior analysis detailed thermal images (FLIR Systems, Inc., 2014; FLIR Systems, Inc., 2018). The thermal camera records infrared radiation, whereupon temperature readings may be obtained through the Stefan–Boltzmann law, which describes the power radiated from a black body in terms of its temperature.

The exit-jet was placed in front of the model eye using a modified metallic rod of 50 cm [Fig. 6]. The thermal camera was fixed onto an adjustable jaws flex clamp mounted with a gooseneck extension tripod standing at a measurable angle slightly less than 90° to the eye.

The separation between the nozzle of the blower and the centre of the model cornea was controlled by a pupilometer. Four different distances were chosen: 0.5 cm, 1 cm, 1.5 cm and 3 cm. A continuous flow of air at room temperature (22˚C) and three different durations was selected using the aesthesiometer control unit: 0.5 s, 1 s and 1.5 s. The stimulus intensity of the air-flow was configured at four different values: 250 unit, 210 unit, 140 unit and 70 unit. These parameters were selected according to aesthesiometry literature [5,11,15]. The footprint size is defined as the diameter in which less than 0.5˚C or 1˚C temperature gradient was measured.

The thermal camera recorded infrared video thermography at 24 Hz for 5 seconds. For each combination of the parameters described above, measurements were repeated three times.

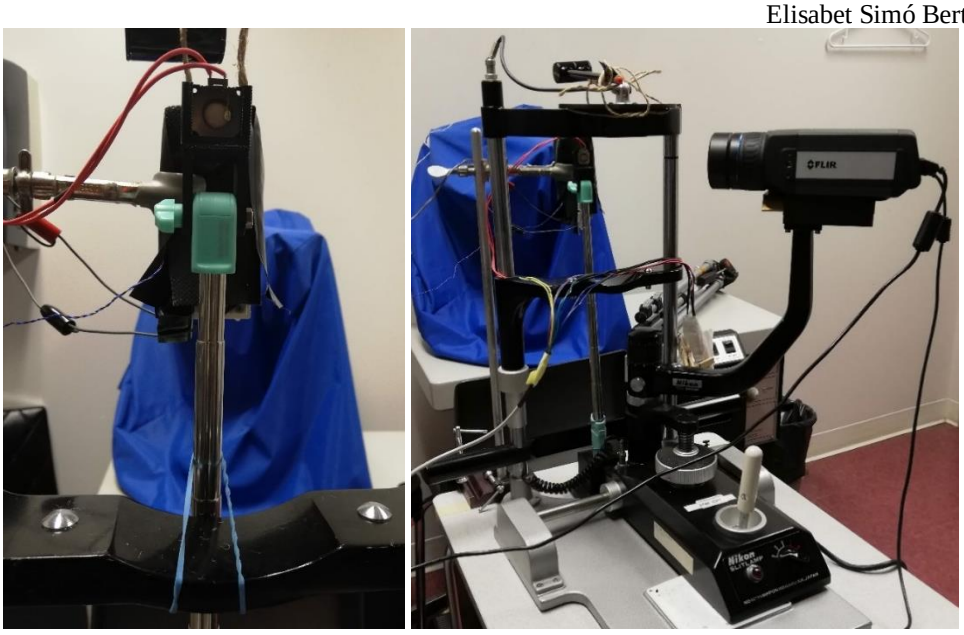

Fig. 5. View from the back of the micro-blower (left) and general view of the thermal camera and model eye experiment set up (right).

For this part of the study, measurements were conducted with and without the brass nozzle and were repeated using the Non-contact corneal aesthesiometer (NCCA) [Fig. 7]. The NCCA used for this comparison was developed by Murphy and co-workers in 1996 and is described in the literature [11]. Briefly, the main differences between the NCCA and the current aesthesiometer design resided in the exit-jet and control unit.

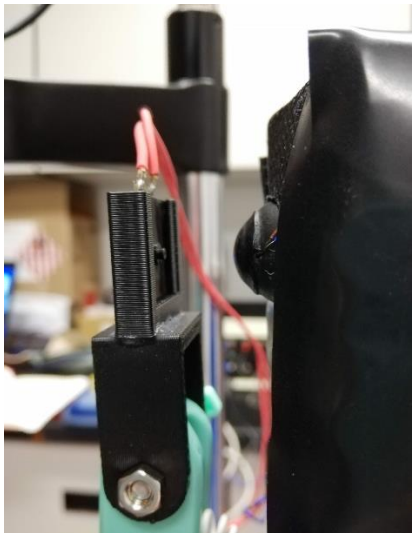

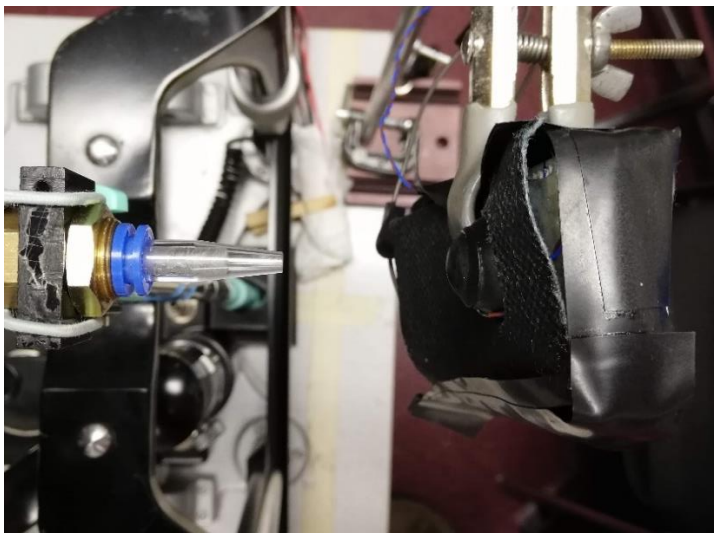

Fig. 6. Micro-blower in front of the model eye. **Fig. 7.** NCCA exit-jet in front of the model eye seen from above.

3. Results

3.1. Force exerted by the jet analysed with a microbalance

Table 1 presents a summary of the results obtained with different intensities of the air-flow, with a duration of 10 s and at distances of 3 and 1.5 cm (the results obtained with the combination of all parameters under study are provided in Annex 1). It may be observed that the standard error of the mean (SEM) for these measurements with the brass nozzle had a small value, in comparison with the value of the mean, thus evidencing the good repeatability of the procedure. On average, microbalance readings (g) increased with the intensity of the air-flow, and when the air-flow was applied at a distance

of 3 cm results were very similar, or slightly higher, than when distance was of 1.5 cm. These results are also shown in Fig. 8.

Intensity (unit)	Average	SEM
250	0.03576	±5.27E-04
210	0.03069	±1.68E-04
140	0.01428	±5.12E-05
70	0.00188	±3.89E-05

Intensity (unit)	Average	SEM
250	0.03939	±5.99E-04
210	0.03278	±4.78E-04
140	0.01532	±1.40E-04
70	0.00205	±2.69E-05

Table 1. Results of the microbalance readings (g) exerted by the air at each intensity tested during 10 seconds at 3 cm (left) and during 10 seconds at 1.5 cm (right).

Plotted in the same graph, the microbalance readings (g) for intensities 250 unit, 210 unit and 140 unit, showed a plateau after obtaining a maximum value, as seen in Fig. 9. It was not possible to know exactly the time (s) when the results reached the maximum value because the recording software did not have enough time resolution. Therefore, to plot the results, three reference times were chosen: A corresponds to one second after obtaining the highest value, B after 5 seconds and C after 10 seconds. The results obtained for intensities of 250 unit and 210 unit were similar but the plateau showed greater stability for an intensity of 210 unit, as may be observed in Fig. 9. With the three intensities at a distance of 3 cm from the microbalance, the maximum microbalance reading (g) was larger and the difference between that maximum value and the value, once stability was reached, was more significant than when measurements were conducted at 1.5 cm. In contrast, results at 1.5 cm and below were more stable.

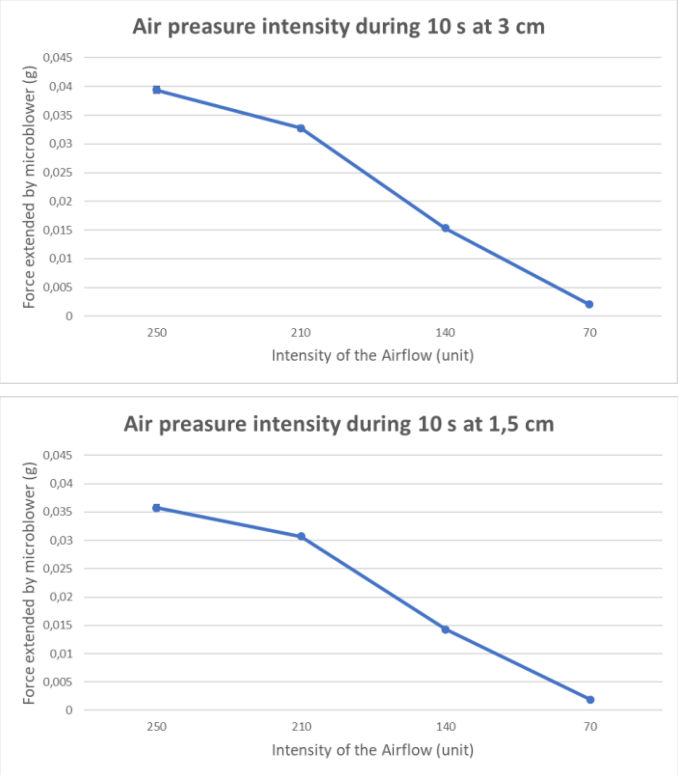

Fig. 8. Results obtained at the different intensities tested for the distance of 3 cm during 10s (top) and for the distance of 1.5 cm during 10 s (bottom).

The experiment could not be repeated at 0.5 cm without the brass nozzle due to the sensibility of the microbalance and the set up of the aesthesiometer. Similarly, the results below 140 unit were not reliable as no noticeable measurement maximum was observed. For measurement times shorter than 5 seconds, the resulting graphics showed a parabolic behaviour and the microbalance readings (g) were slightly smaller. The microbalance readings (g) exerted by the micro-blower without the nozzle were higher than with the brass nozzle adapted, as the exit diameters were different.

All the results not shown in the graphics may be accessed in Annex 1.

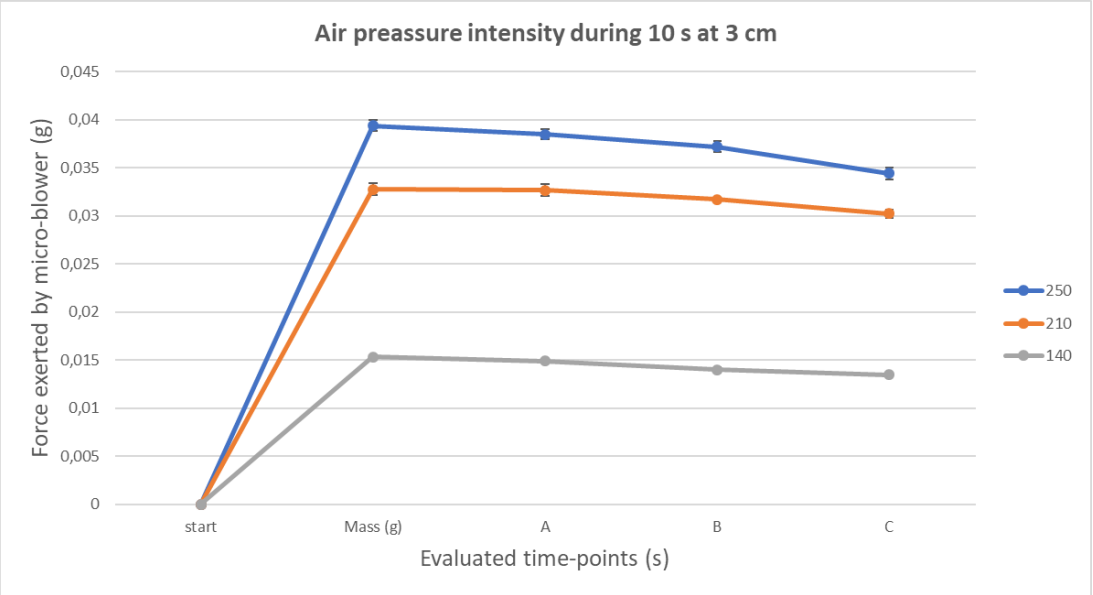

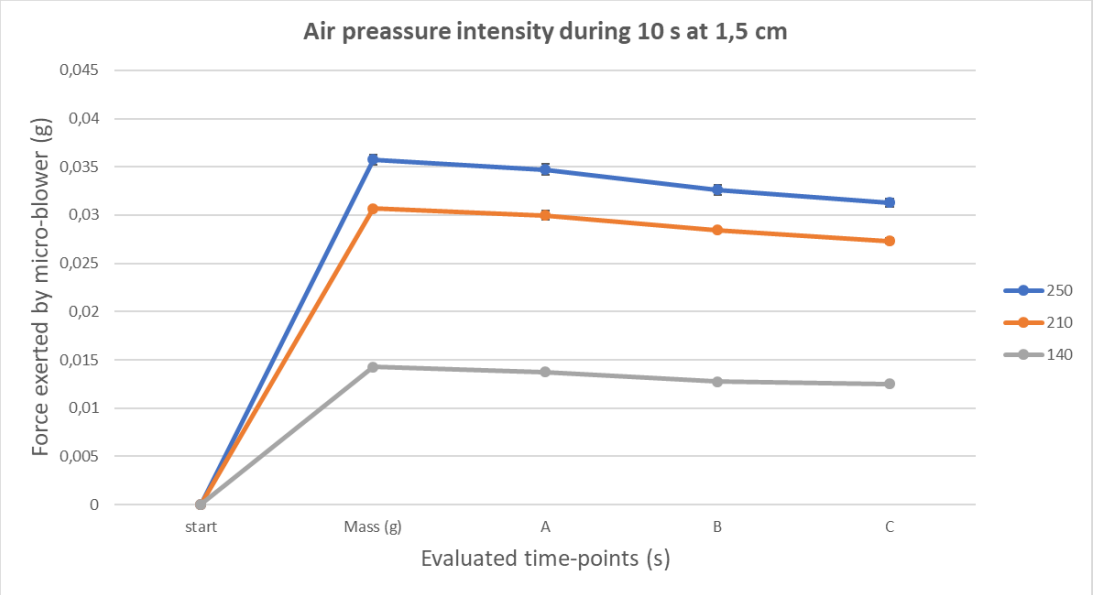

Fig. 9. Comparison of the stability of the microbalance readings (g) exerted by the micro-blower with intensities 250 unit, 210 unit and 140 unit during 10 s at 3 cm trial (top) and 1.5 cm trial (bottom).

3.2. Pattern of the air-flow

The mean of the diameters measured for each intensity and distances during 1.5 s are shown in Fig. 10. The SEM for these measurements were always between ±0.01 and ±0.13. It may be observed that the diameter of the craters is larger without the brass nozzle adapted on the exit-jet. For both experiments, with and without the brass nozzle, the diameter increased when the intensity was higher and when the distance was shorter between the air jet and the powder. This pattern was only partially reversed at the experimental condition with brass nozzle and 250 unit pressure. It must be noted that not all stimulus pressures caused displacement of the powder, particularly at the lower pressures, and measurements were taken only when a definite crater was seen by the examiner.

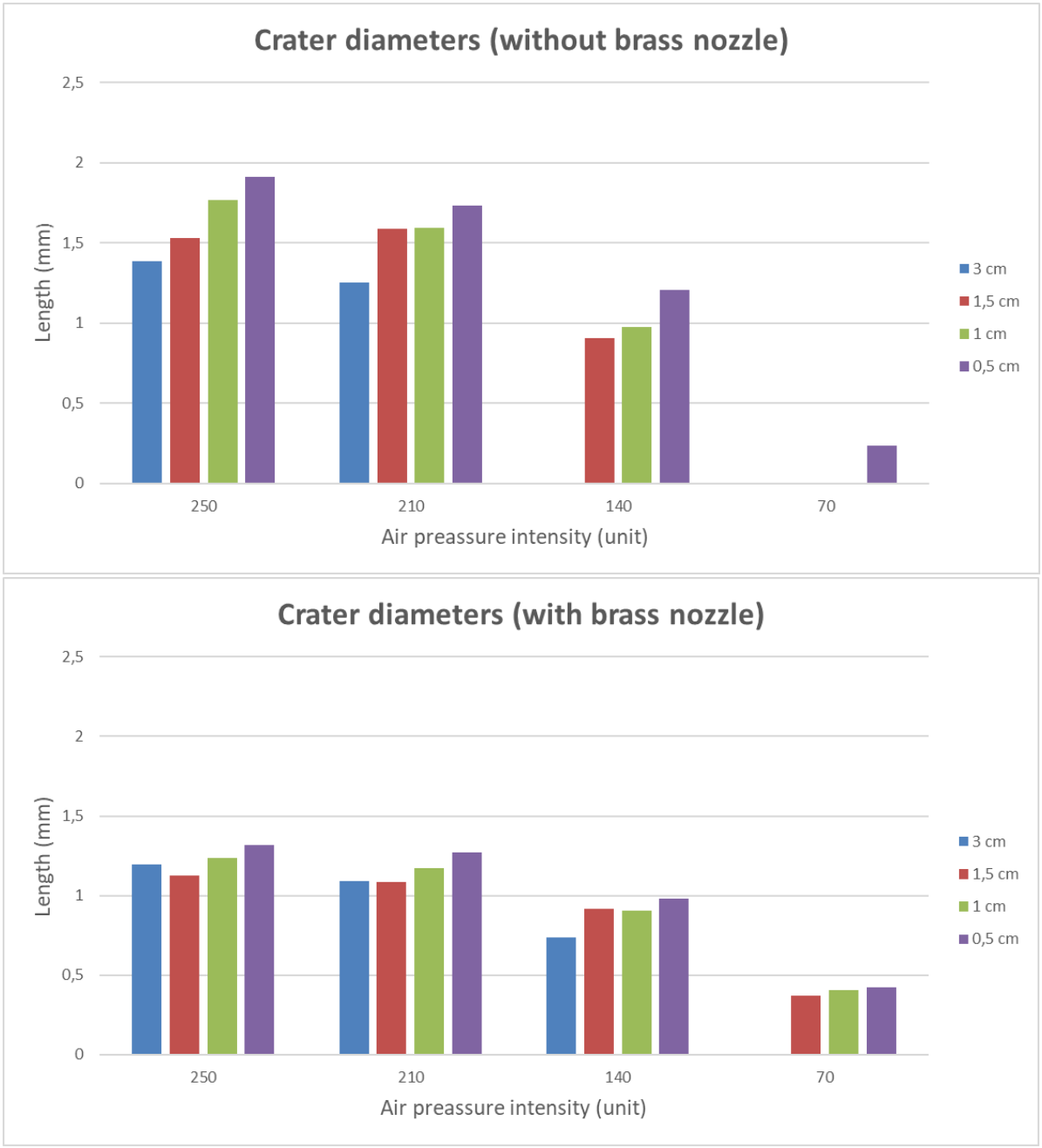

Fig. 10. Diameter of the craters drawn on the lycopodium powder by the air-flow during 1.5 s and various distances, without the adapted brass nozzle (top) and with the adapted brass nozzle (bottom).

The rest of the results are summarized in Annex 2. It may be observed that, in average, the measured diameters for an air-flow time of 0.9 s were slightly smaller than the results showed above but the error margins were larger (between ±0.01 and ±0.36) and the whole results were more unstable.

Regarding the air-flow visualization experiment, it was found that the length of the dust plume increased with the distance of the flow, as it may be seen in table 2. Three marks were defined to measure the diameter of the plume by the division of the selected length in 3 parts. At high air-flow intensities and times of 10 seconds, the dust plume reached a lower altitude than at 140 unit, but they had larger diameters, that is, dust spread more. The maximum diameters with not significant changes were obtained at high intensities and different stimulus durations. In contrast, at 140 unit results were more different.

Stimulus Intensity (unit)	Duration (s)	Average tall mark 1 (cm)	SEM	Average tall mark 2 (cm)	SEM	Average tall mark 3 (cm)	SEM
250	1	0.647	0.018	1.541	0.019	2.557	0.018
250	10	1.071	0.027	2.768	0.023	4.073	0.023
210	10	1.512	0.022	3.291	0.025	4.493	0.023
140	1	0.765	0.018	1.769	0.018	2.781	0.018
140	10	1.215	0.019	3.306	0.090	4.846	0.022

Stimulus Intensity (unit)	Duration (s)	Average Diameter mark 1 (cm)	SEM	Average diameter mark 2 (cm)	SEM	Average diameter mark 3 (cm)	SEM
250	1	0.150	0.008	0.231	0.010	0.356	0.009
250	10	0.230	0.003	0.277	0.009	0.371	0.005
210	10	0.212	0.005	0.294	0.007	0.363	0.011
140	1	0.128	0.003	0.180	0.005	0.222	0.016
140	10	0.204	0.007	0.253	0.006	0.313	0.008

Table 2. Lateral air pattern visualization measurements of each intensity and time tested. Mean diameter (bottom) and mean altitude of the dust plume (top).

3.3. Footprint size of the air-flow stimulus examined with a model eye and a thermal camera

The mean (± error) footprint size (mm) found for each stimulus pressure (unit) and for each distance (cm), tested with 1 s air-flow duration, are shown in Fig. 11. The footprint size was defined as the diameter in which less than 0.5˚C or 1˚C temperature gradient was measured. In agreement with the air-flow visualization experiment, the larger the distance between the eye and the micro-blower, the larger the diameter of corresponding thermal footprint. Smaller diameters were obtained with the lower intensity value at each trial (70 unit).

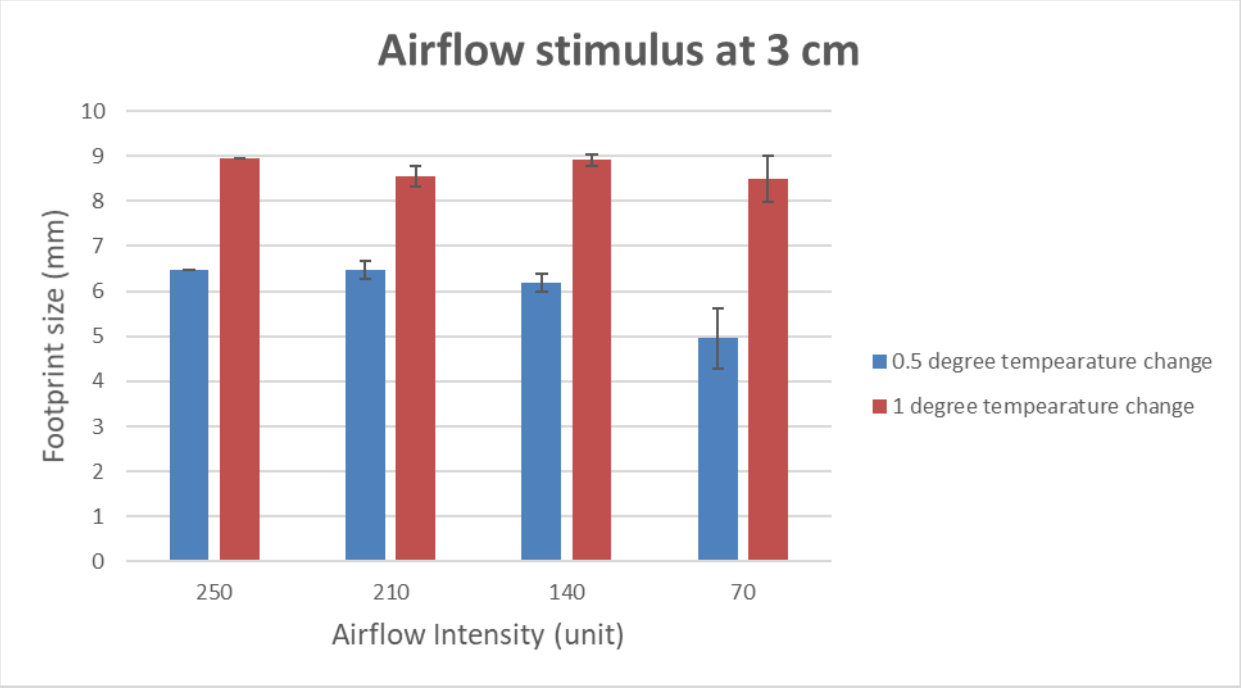

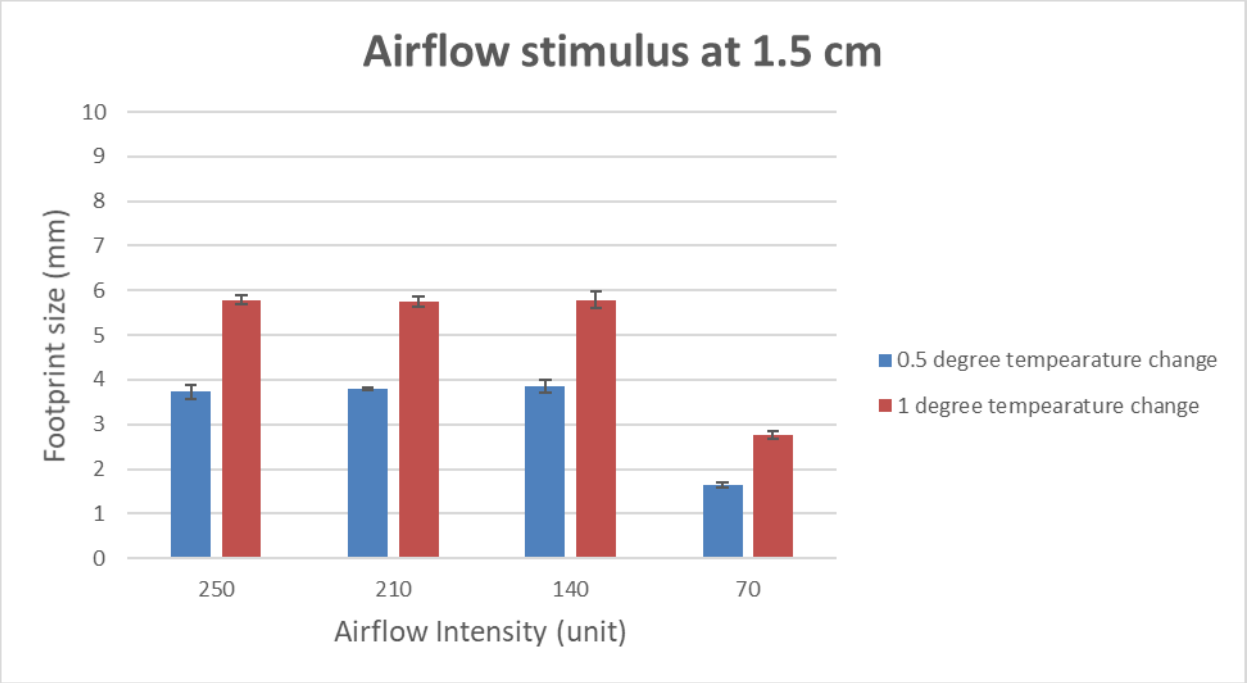

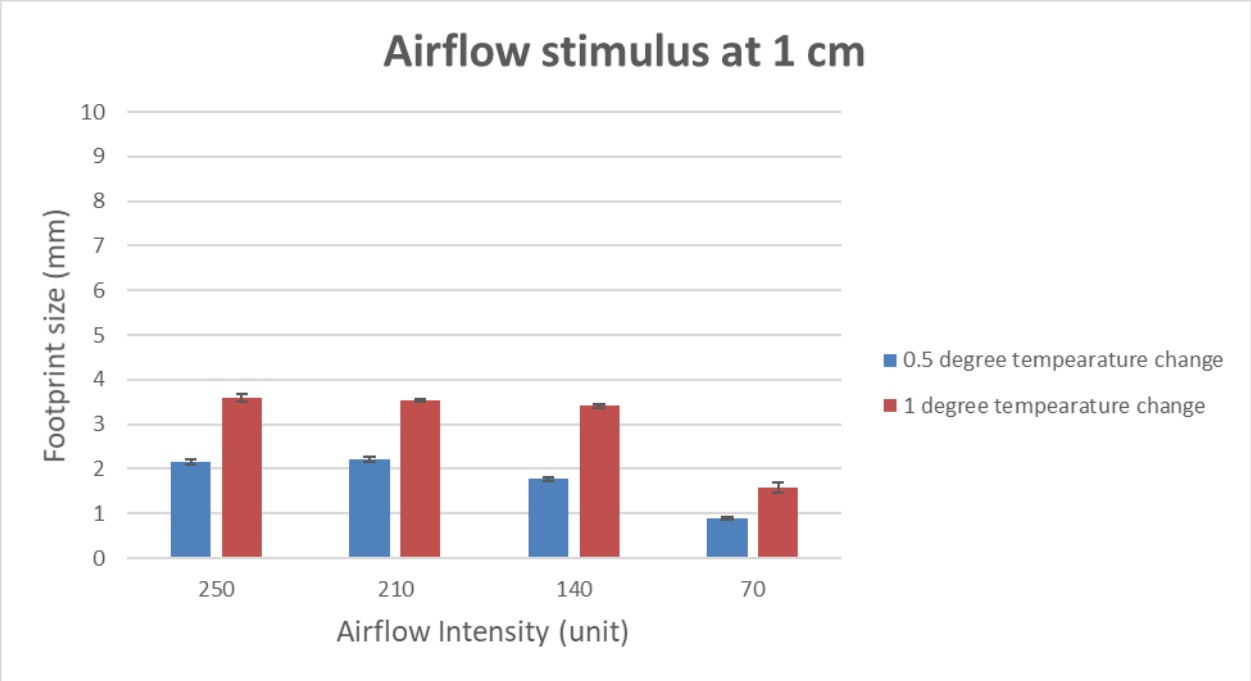

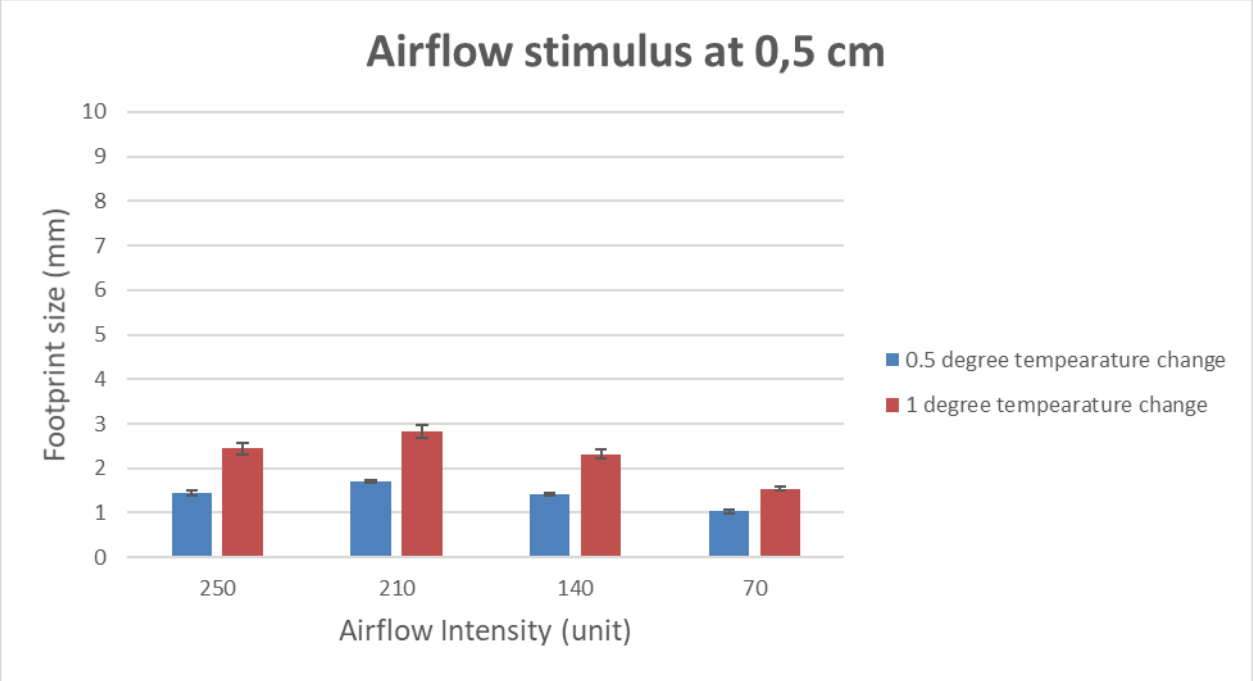

Fig. 11. Diameter (mm) of the temperature footprint produced during 1 second for every intensity (unit) evaluated and at each test distance (cm). These values were taken during the maximum thermal difference.

Full results with the combination of all parameters under study are presented in Annex 3. The temperature of the model eye reached 32.17˚C. Overall, as the intensity was reduced, temperature measurements stayed higher, only decreasing 1.77˚C (trial 70 unit, during 1 s at 3 cm). In contrast, temperature was lower, decreasing 2.83˚C, when distance was reduced (trial 70 unit, during 1 s at 0.5 cm). The air-flow stimulus appears more controlled with the brass nozzle adapted on the exit-jet of the aesthesiometer than in the trials without it.

The diameter results were taken from thermic profile plots like the examples shown in Fig. 12, transforming the pixels to millimetres. As may be observed from these figures, the pink lines drawn where the diameter values corresponding to the 0.1˚C, 0.5˚C and 1˚C temperature gradients. Thermography plots showed that temperature changes induced by air at room temperature were always larger in the center of the model cornea and smaller towards the corneal borders

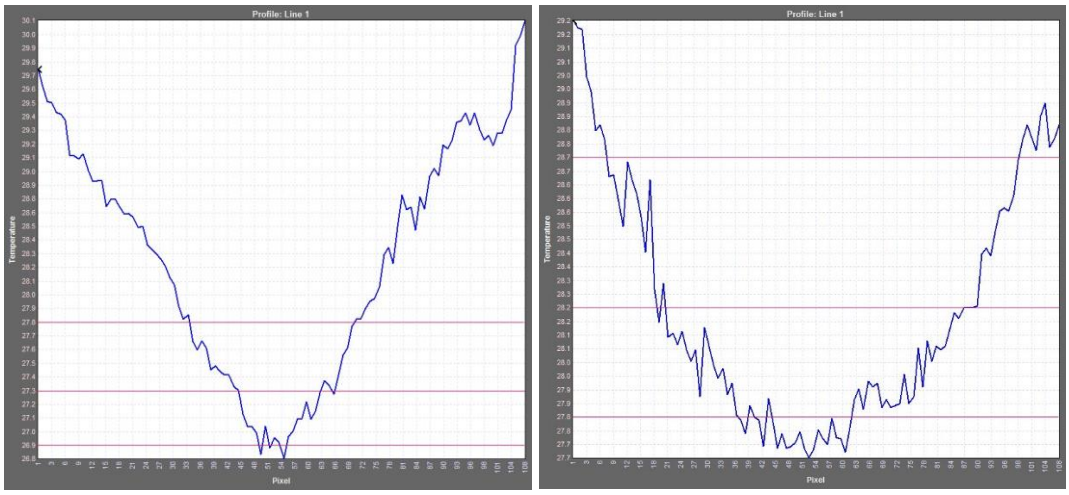

Fig.12. Profile plots saved from FLIR ResearchIR Max Version 4.30.1.70 software. Footprint diameter results (in pixels) at 210 unit during 1s test at 1 cm (left) and 3 cm (right). These values were taken during the maximum thermal difference.

4.Discussion

This research is included in a main project leading to a PhD thesis at the University of Waterloo (Canada) called *Studies on corneal sensitivity*. The aim of the work was to gain a better understanding of corneal sensitivity by improving its way of evaluation. The objective of the study was to determine the optimal parameters of the air jet of a new non-contact corneal aesthesiometer and to explore the temperature change caused by this device.

The stability of the force exerted by the air jet was determined with the **microbalance experiment**. With the trials where the stimulus duration was 10 seconds, a well defined plateau was observed, although this test duration was only for visualisation purposes, not for trials *in vivo.* Besides, confirming previous reports [11,16], the maximum measured force (g) was similar for all time trials (10 s and 1 s) and test distances. In contrast, the largest change in maximum force was found between different intensities. However, as the normal cornea is able to detect stimuli with lower intensities than 250 unit [13], future *in vivo* measurements are required to determine the optimal intensity values for the new aesthesiometer. In addition, a stimulus duration of 1 s was sufficient to reach the maximum force, in agreement with published literature [18], which suggests this duration as optimal for *in vivo* measurements. In effect, corneal nerves respond to the initial impact of the air-pulse on the corneal surface, rather than to the actual volume of air in the stimulus pulse [18].

The results showed that with the 0.5 mm air-jet brass nozzle the force was smaller than without the nozzle (0.75 mm air-jet). This small difference between the diameters of the exit-jet could produce a difference with the dispersion of the air-flow directed to the surface of the microbalance, resulting in larger values (g). Nevertheless, for the best performance of the micro-blower we suggest using the brass nozzle in the new aesthesiometer, as with this configuration the smallest diameter of stimulation was found. From the results displayed in Figure 8 and 9, it may be observed that the best outcome was obtained with a distance of 1.5 cm.

The technique of recording the results needs to be improved because some interesting measures were lost, like the exact time the air-flow reached the maximum value (g). It is known that this time is less than 1 s [15], but the exact value is as yet undetermined, even considering its relevance for *in vivo* trials. Finally, some problems were also found with the 0.5 cm trial without the nozzle because of the set up of the microbalance and aesthesiometer having a negative impact on the microbalance sensitivity.

With the pattern of the air-flow using lycopodium powder in the **lycopodium powder displacement test**, the expected results were that the diameter of the craters would increase with the intensity of the stimulus. The measurements confirmed this initial hypothesis. However, it was also expected to find a more significant powder displacement when the distances between the air jet and the powder surface increased, which the results did not show. With the no nozzle test, the diameter was clearly larger when the distance of the test increased, whereas for the brass nozzle trials the working distances and the stimulus duration did not appear to create relevant changes in the displacement results. One improvement of the design of this experiment could be the control over the thickness of the lycopodium powder layer over all the surface, a factor that might have altered the results.

In addition, the **air flow pattern** showed a gradual dispersion of the lycopodium powder, as was expected. However, the pattern of the air observed in this experiment may not necessarily replicate the *in vivo* conditions on the corneal surface, which is covered by a thin tear film layer. The best distance for the study was not well defined in this case. However, from the results summarized in Table 2, it may be

evidenced an optimal air pressure of 140 unit, with which the diameter of the dust plume was always the smallest, irrespective of the duration of the stimulus, that is, less dispersion occurred.

Lastly, with the **thermal camera** the measurements have shown that the air-flow produced a well defined pattern of reduction of the temperature on the model cornea. Two aspects may be discussed in this regard: which was the temperature change of the corneal surface and which diameter of the cornea was affected, so the cornea may be stimulated mechanically and thermally in accordance with previous reports [16].

In our case, the continuous flow of air at room temperature (22˚C) touched the model eye corneal surface (29.84±2.34˚C) and its temperature decreased without evaporation due to the lack of tear film. In a real case, the literature indicates that normal ocular surface temperature ranges from 32.9 to 36˚C [19]. Because of the tear film, which is a good heat conductor, the footprint size found in a real-life experiment should be larger than the value found in this experiment, although the actual results may depend on the tear quality of the subject so that a future trial *in vivo* should include both healthy subjects and subjects with dry eye disease.

Other interesting findings of this experiment were, as it is shown on the results and coinciding with the other parts of the research, that the stimulus duration did not affect the thermal pattern and that the temperature gradient across the surface remained constant for the duration of the stimulus. Once the air-flow was interrupted, the temperature of the surface gradually recovered its previous baseline values.

Secondly, the working distances were related to the footprint size as it was found in the air-flow pattern experiment: at long distances between the model eye and the exit jet the diameter was larger and this value decreased as distances shortened. Thirdly, the intensity did not have any relation with the diameter values but only with small changes in temperature. The highest intensities resulted in a more significant decrease in corneal temperature than low intensities.

Finally, the results can confirm that the area of cooling produced by the air-flow was localised during the trials. Unlike reported by previous authors [13,15], thermography images done by Belmonte and their colleagues on their research in 1999 showed that temperature changes induced by air at room temperature were always restricted to the center of the cornea and did not extend to the corneal borders too [16]. However, the aesthesiometer footprint is larger than that of the Cochet-Bonnet device and stimulates a less specific number of sensory receptors [5], so in this research we aim at a smaller diameter. From the results shown in Figure 11, the best parameters may be a yet undetermined intensity applied at a 1 cm distance and during 1 second.

5. Conclusion

Although further work is necessary to determine the optimal parameters of the air-jet of the aesthesiometer, an association was found between the diameter of the powder displacement and the footprint size found with the thermal camera. The tree experiments have results in common: the distance and the duration of the stimulus is not the cause of the variation of the diameter, leaving intensity as the most important parameter. However, more information and repeated trials are needed to have clear results for the improvement of the new device. The characterisation of the new device units is also necessary for the comparison between studies, although there is still no consistency in stimulus parameters used in the published literature [8,13,15,20,21]. Overall, as previously documented [22,23], infrared thermography may be considered a good imaging modality to study the ocular surface temperature.

6. Limitations and future work

The general limitations found in the present research were that this was the beginning of a larger project still unfinished and we could not do the research *in vivo.* For the microbalance experiment, we should find a better way of recording the results, which may allow finding a relation between force and time. For the lycopodium powder, to have a control over the dust thickness and to determine the error with the craters. Finally, with the thermal camera experiment, to repeat the procedures with the instillation of saline or tear substitutes on the model eye before the trials.

7. References

[1] Millodot M. A review of research on the sensitivity of the cornea. Ophthal Physl Opt 1984; 4: 305–318. https://doi.org/10.1111/j.1475-1313.1984.tb00372.x

[2] Oliveira-Soto L, Efron N. Morphology of corneal nerves using confocal microscopy. Cornea 2001; 20: 374–384.

[3] Marfurt CF, Cox J, Deek S, Dvorscak L. Anatomy of the human corneal innervations. Exp Eye Res 2010; 90: 478–492.

[4] Labbé A, Alalwani H, Van Went C, Brasnu E, Georgescu D, Baudouin C. The relationship between subbasal nerve morphology and corneal sensation in ocular surface disease. Invest Ophthalmol Vis 2012; 53: 4926–4931. https://doi.org/10.1167/iovs.11-8708

[5] Lum E, Golebiowski B, Gunn R, Babhoota M, Swarbrick H. Corneal sensitivity with contact lenses of different mechanical properties. Optometry Vision Sci 2013; 90: 954–960. https://doi.org/10.1097/OPX.0000000000000016

[6] Golebiowski B, Papas E, Stapleton F. Corneal mechanical sensitivity measurement using a staircase technique. Ophthal Physl Opt 2005; 25: 246–253. https://doi.org/10.1111/j.1475-1313.2005.00295.x

[7] Müller LJ, Marfurt CF, Kruse F, Tervo TMT. Corneal nerves: Structure, contents and function. Exp Eye Res 2003; 76: 521–542. https://doi.org/10.1016/S0014-4835(03)00050-2

[8] Stapleton F, Tan ME, Papas EB, Ehrmann K, Golebiowski B, Vega J, Holden BA. Corneal and conjunctival sensitivity to air stimuli. Brit J Ophthalmol 2004; 88: 1547–1551. https://doi.org/10.1136/bjo.2004.044024

[9] Stapleton F, Marfurt C, Golebiowski B, Rosenblatt M, Bereiter D, Begley C, Dartt D, Gallar J, Belmonte C, Hamrah P, Willcox M. The TFOS International Workshop on Contact Lens Discomfort: Report of the subcommittee on neurobiology. Invest Ophthalmol Vis Sci 2013; 54: TFOS71-TFOS97. https://doi.org/10.1167/iovs.13-13226

[10] Kaido M, Kawashima M, Ishida R, Tsubota K. Relationship of corneal pain sensitivity with dry eye symptoms in dry eye with short tear break-up time. Invest Ophthalmol Vis Sci 2016; 57: 914–919. https://doi.org/10.1167/iovs.15-18447

[11]Murphy PJ, Patel S, Marshall J. A new non-contact corneal aesthesiometer (NCCA). Ophthal Physl Opt 1996; 16: 101–107. https://doi.org/10.1016/0275-5408(95)00102-6

[12]Golebiowski B, Papas E, Stapleton F. Assessing the sensory function of the ocular surface: Implications of use of a non-contact air jet aesthesiometer versus the Cochet-Bonnet aesthesiometer. Exp Eye Res 2011; 92: 408–413. https://doi.org/10.1016/j.exer.2011.02.016

[13]Nosch DS, Pult H, Albon J, Purslow C, Murphy PJ. Does air gas aesthesiometry generate a true mechanical stimulus for corneal sensitivity measurement? Clin Exp Optom 2017; 101: 193–199. https://doi.org/10.1111/cxo.12603

[14]Feng Y, Simpson TL. Nociceptive sensation and sensitivity evoked from human cornea and conjunctiva stimulated by CO_2. Invest Ophthalmol Vis Sci 2003; 44: 529–532. https://doi.org/10.1167/iovs.02-0003

[15]Murphy PJ, Morgan PB, Patel S, Marshall J. Corneal surface temperature change as the mode of stimulation of the Non-Contact Corneal Aesthesiometer. Cornea 1999; 18: 333–342.

[16]Belmonte C, Acosta MC, Schmelz M, Gallar J. Measurement of corneal sensitivity to mechanical and chemical stimulation with a CO_2 esthesiometer. Invest Ophthalm Vis Sci 1999; 40: 513–519.

[17]Vega JA, Simpson TL, Fonn D. A noncontact pneumatic esthesiometer for measurement of ocular sensitivity: A preliminary report. Cornea 1999. 18: 675–681. https://doi.org/10.1097/00003226-199911000-00009

[18]Murphy PJ, Lawrenson JG, Patel S, Marshall J. Reliability of the Non-Contact Corneal Aesthesiometer and its comparison with the Cochet-Bonnet aesthesiometer. Ophthal Physl Opt 1998; 18: 532-539.

[19]Purslow C, Wolffsohn JS. Ocular surface temperature: A review. Eye Contact Lens 2005; 31: 117–123. https://doi.org/10.1097/01.ICL.0000141921.80061.17

[20]Situ P, Simpson TL, Jones LW, Fonn D. Effects of silicone hydrogel contact lens wear on ocular surface sensitivity to tactile, pneumatic mechanical, and chemical stimulation. Invest Ophthalmol Vis Sci 2010; 51: 6111–6117. https://doi.org/10.1167/iovs.09-4807

[21]Gallar J, Tervo TMT, Neira W, Holopainen JM, Lamberg ME, Miñana F, Acosta MC, Belmonte C. Selective changes in human corneal sensation associated with herpes simplex virus keratitis. Invest Ophth Vis Sci 2010; 51: 4516–4522. https://doi.org/10.1167/iovs.10-5225

[22]Tan L, Cai ZQ, Lai NS. Accuracy and sensitivity of the dynamic ocular thermography and inter-subjects ocular surface temperature (OST) in Chinese young adults. Contact Lens Anterio 2009; 32: 78–83.

[23]Tan JH, Ng EYK, Acharya UR. Evaluation of topographical variation in ocular surface temperature by functional infrared thermography. Infrared Phys Techn 2011; 54: 469–477. https://doi.org/10.1016/j.infrared.2011.07.010

8. Annex

8.1. Annex 1

Microbalance results (g)												
Brass Nozzle	**Trial 1**	**Trial 2**	**Trial 3**	**Trial 4**	**Trial 5**	**Trial 6**	**Trial 7**	**Trial 8**	**Trial 9**	**Trial 10**	**Average**	**SEM**
250, 10s, 3cm	0,043	0,040	0,042	0,037	0,041	0,038	0,040	0,039	0,038	0,038	0,039	5,993E-04
210, 10s, 3cm	0,035	0,034	0,033	0,034	0,034	0,032	0,031	0,030	0,032	0,034	0,033	4,779E-04
140, 10s, 3cm	0,016	0,016	0,015	0,016	0,015	0,015	0,016	0,016	0,014	0,015	0,015	1,397E-04
70, 10s, 3cm	0,002	0,002	0,002	0,002	0,002	0,002	0,002	0,002	0,002	0,002	0,002	2,687E-05
250, 10s, 1.5cm	0,037	0,037	0,039	0,036	0,035	0,036	0,034	0,036	0,034	0,034	0,036	5,271E-04
210, 10s, 1.5cm	0,032	0,031	0,030	0,031	0,031	0,031	0,031	0,030	0,031	0,030	0,031	1,676E-04
140, 10s, 1.5cm	0,015	0,014	0,014	0,014	0,014	0,014	0,014	0,014	0,015	0,014	0,014	5,121E-05
70, 10s, 1.5cm	0,002	0,002	0,002	0,002	0,002	0,002	0,002	0,002	0,002	0,002	0,002	3,887E-05
250, 10s, 1cm	0,038	0,034	0,034	0,033	0,033	0,033	0,033	0,034	0,034	0,033	0,034	4,387E-04
210, 10s, 1cm	0,031	0,029	0,029	0,031	0,030	0,029	0,029	0,031	0,030	0,029	0,030	2,221E-04
140, 10s, 1cm	0,014	0,014	0,014	0,014	0,015	0,014	0,014	0,014	0,014	0,014	0,014	6,360E-05
70, 10s, 1cm	0,002	0,002	0,002	0,002	0,002	0,002	0,002	0,002	0,002	0,021	0,004	1,889E-03
250, 10s, 0.5cm	0,035	0,035	0,035	0,032	0,031	0,031	0,030	0,032	0,032	0,031	0,032	5,556E-04
210, 10s, 0.5cm	0,029	0,028	0,027	0,029	0,030	0,028	0,028	0,029	0,028	0,028	0,028	2,409E-04
140, 10s, 0.5cm	0,014	0,014	0,014	0,013	0,013	0,014	0,013	0,014	0,014	0,013	0,014	8,667E-05
70, 10s, 0.5cm	0,002	0,002	0,002	0,002	0,002	0,002	0,002	0,002	0,002	0,002	0,002	1,795E-05
250, 5s, 3cm	0,040	0,040	0,038	0,040	0,042	0,041	0,040	0,040	0,040	0,041	0,040	3,538E-04
210, 5s, 3cm	0,036	0,035	0,034	0,035	0,034	0,035	0,034	0,034	0,036	0,035	0,035	2,187E-04
140, 5s, 3cm	0,016	0,016	0,017	0,016	0,016	0,016	0,016	0,016	0,016	0,017	0,016	9,568E-05
70, 5s, 3cm	0,002	0,002	0,002	0,002	0,002	0,002	0,002	0,002	0,002	0,002	0,002	2,134E-05
250, 5s, 1.5cm	0,039	0,036	0,037	0,036	0,035	0,036	0,036	0,035	0,036	0,036	0,036	3,459E-04
210, 5s, 1.5cm	0,034	0,032	0,031	0,032	0,032	0,031	0,031	0,032	0,031	0,032	0,032	2,488E-04
140, 5s, 1.5cm	0,015	0,015	0,015	0,015	0,015	0,015	0,015	0,015	0,015	0,015	0,015	7,860E-05
70, 5s, 1.5cm	0,002	0,002	0,002	0,002	0,002	0,002	0,002	0,002	0,002	0,002	0,002	2,906E-05
250, 5s, 1cm	0,038	0,036	0,037	0,035	0,035	0,035	0,036	0,035	0,035	0,034	0,035	3,489E-04
210, 5s, 1cm	0,032	0,031	0,032	0,031	0,031	0,031	0,032	0,031	0,032	0,032	0,031	1,748E-04
140, 5s, 1cm	0,015	0,015	0,015	0,016	0,015	0,015	0,015	0,015	0,015	0,015	0,015	1,106E-04
70, 5s, 1cm	0,002	0,002	0,002	0,002	0,002	0,002	0,002	0,002	0,002	0,002	0,002	2,134E-05
250, 5s, 0.5cm	0,035	0,033	0,033	0,033	0,033	0,033	0,034	0,033	0,033	0,033	0,033	2,308E-04
210, 5s, 0.5cm	0,030	0,029	0,029	0,029	0,029	0,029	0,029	0,028	0,030	0,028	0,029	1,345E-04
140, 5s, 0.5cm	0,014	0,014	0,014	0,014	0,014	0,014	0,014	0,014	0,014	0,014	0,014	6,633E-05
70, 5s, 0.5cm	0,002	0,002	0,002	0,002	0,002	0,002	0,002	0,002	0,002	0,002	0,002	1,667E-05
250, 1.5s, 3cm	0,044	0,040	0,041	0,041	0,040	0,040	0,043	0,042	0,041	0,040	0,041	4,069E-04
210, 1.5s, 3cm	0,036	0,035	0,035	0,035	0,035	0,035	0,037	0,034	0,035	0,035	0,035	2,000E-04
140, 1.5s, 3cm	0,016	0,016	0,017	0,016	0,016	0,016	0,016	0,016	0,016	0,017	0,016	1,023E-04
70, 1.5s, 3cm	0,002	0,002	0,002	0,002	0,002	0,002	0,002	0,002	0,002	0,002	0,002	2,494E-05
250, 1.5s, 1.5cm	0,039	0,037	0,037	0,037	0,038	0,037	0,037	0,037	0,036	0,037	0,037	2,108E-04
210, 1.5s, 1.5cm	0,033	0,032	0,033	0,032	0,033	0,033	0,032	0,032	0,032	0,032	0,032	1,511E-04
140, 1.5s, 1.5cm	0,015	0,015	0,015	0,015	0,015	0,015	0,015	0,015	0,015	0,015	0,015	6,227E-05
70, 1.5s, 1.5cm	0,002	0,002	0,002	0,002	0,002	0,002	0,002	0,002	0,002	0,002	0,002	3,350E-05
250, 1.5s, 1cm	0,038	0,036	0,036	0,036	0,036	0,037	0,036	0,035	0,036	0,035	0,036	2,399E-04
210, 1.5s, 1cm	0,033	0,032	0,032	0,031	0,032	0,032	0,032	0,032	0,032	0,032	0,032	9,667E-05
140, 1.5s, 1cm	0,016	0,015	0,015	0,015	0,015	0,015	0,015	0,015	0,015	0,015	0,015	4,726E-05
70, 1.5s, 1cm	0,002	0,002	0,002	0,002	0,002	0,002	0,002	0,002	0,002	0,002	0,002	2,134E-05
250, 1.5s, 0.5cm	0,035	0,034	0,032	0,033	0,033	0,033	0,033	0,033	0,033	0,033	0,033	2,121E-04
210, 1.5s, 0.5cm	0,030	0,029	0,030	0,030	0,030	0,029	0,029	0,029	0,029	0,029	0,030	1,186E-04
140, 1.5s, 0.5cm	0,014	0,014	0,014	0,014	0,014	0,014	0,014	0,014	0,014	0,014	0,014	6,872E-05
70, 1.5s, 0.5cm	0,002	0,002	0,002	0,002	0,002	0,002	0,002	0,002	0,002	0,002	0,002	1,795E-05
250, 1s, 3cm	0,044	0,040	0,040	0,041	0,040	0,040	0,043	0,042	0,041	0,040	0,041	4,126E-04
210, 1s, 3cm	0,036	0,035	0,035	0,035	0,035	0,035	0,037	0,034	0,035	0,035	0,035	2,004E-04
140, 1s, 3cm	0,017	0,017	0,017	0,017	0,017	0,017	0,017	0,017	0,017	0,016	0,017	7,491E-05
70, 1s, 3cm	0,002	0,002	0,002	0,002	0,002	0,002	0,002	0,002	0,002	0,002	0,002	2,000E-05
250, 1s, 1.5cm	0,040	0,037	0,037	0,037	0,038	0,068	0,037	0,037	0,037	0,037	0,040	3,065E-03
210, 1s, 1.5cm	0,034	0,032	0,032	0,033	0,032	0,033	0,032	0,033	0,032	0,033	0,033	1,903E-04
140, 1s, 1.5cm	0,016	0,015	0,015	0,015	0,016	0,015	0,015	0,014	0,016	0,015	0,015	1,265E-04
70, 1s, 1.5cm	0,001	0,002	0,001	0,002	0,001	0,001	0,001	0,002	0,001	0,001	0,001	9,574E-05
250, 1s, 1cm	0,038	0,037	0,036	0,036	0,035	0,036	0,036	0,036	0,035	0,036	0,036	2,429E-04
210, 1s, 1cm	0,033	0,032	0,032	0,032	0,032	0,032	0,032	0,033	0,032	0,032	0,032	8,876E-05
140, 1s, 1cm	0,016	0,016	0,015	0,015	0,015	0,015	0,015	0,015	0,016	0,015	0,015	9,894E-05
70, 1s, 1cm	0,002	0,002	0,001	0,002	0,002	0,002	0,002	0,001	0,002	0,001	0,002	9,195E-05
250, 1s, 0.5cm	0,034	0,033	0,033	0,033	0,032	0,033	0,033	0,033	0,032	0,033	0,033	1,599E-04
210, 1s, 0.5cm	0,029	0,029	0,029	0,029	0,029	0,029	0,028	0,030	0,029	0,029	0,029	1,055E-04
140, 1s, 0.5cm	0,014	0,014	0,014	0,014	0,014	0,014	0,014	0,014	0,014	0,014	0,014	4,472E-05
70, 1s, 0.5cm	0,002	0,001	0,001	0,002	0,001	0,001	0,001	0,001	0,001	0,001	0,001	1,000E-04

Microbalance results (g)												
No Nozzle	Trial 1	Trial 2	Trial 3	Trial 4	Trial 5	Trial 6	Trial 7	Trial 8	Trial 9	Trial 10	Average	SEM
250, 10s, 3cm	0,104	0,099	0,096	0,101	0,096	0,094	0,093	0,090	0,099	0,094	0,097	1,296E-03
210, 10s, 3cm	0,087	0,086	0,084	0,083	0,088	0,089	0,087	0,085	0,084	0,083	0,086	6,605E-04
140, 10s, 3cm	0,045	0,043	0,044	0,043	0,043	0,043	0,045	0,045	0,044	0,043	0,044	3,505E-04
70, 10s, 3cm	0,008	0,007	0,007	0,007	0,008	0,008	0,007	0,008	0,008	0,007	0,007	6,110E-05
250, 10s, 1.5cm	0,083	0,075	0,078	0,082	0,079	0,078	0,081	0,081	0,077	0,082	0,079	7,866E-04
210, 10s, 1.5cm	0,072	0,068	0,068	0,071	0,067	0,071	0,067	0,072	0,069	0,068	0,069	6,471E-04
140, 10s, 1.5cm	0,037	0,035	0,037	0,036	0,037	0,038	0,036	0,036	0,035	0,036	0,036	2,432E-04
70, 10s, 1.5cm	0,007	0,006	0,006	0,006	0,006	0,006	0,007	0,007	0,007	0,007	0,006	3,416E-05
250, 10s, 1cm	0,066	0,064	0,062	0,061	0,062	0,063	0,061	0,064	0,062	0,062	0,063	5,525E-04
210, 10s, 1cm	0,059	0,057	0,056	0,055	0,054	0,053	0,055	0,054	0,055	0,055	0,055	5,182E-04
140, 10s, 1cm	0,034	0,034	0,033	0,033	0,035	0,033	0,034	0,033	0,033	0,034	0,034	1,698E-04
70, 10s, 1cm	0,006	0,006	0,006	0,006	0,006	0,006	0,006	0,006	0,006	0,006	0,006	3,590E-05
250, 5s, 3cm	0,104	0,096	0,096	0,094	0,093	0,100	0,100	0,098	0,096	0,096	0,097	1,045E-03
210, 5s, 3cm	0,088	0,086	0,086	0,087	0,088	0,087	0,086	0,088	0,086	0,085	0,087	3,321E-04
140, 5s, 3cm	0,046	0,045	0,043	0,044	0,047	0,046	0,046	0,046	0,044	0,045	0,045	4,058E-04
70, 5s, 3cm	0,008	0,007	0,008	0,007	0,008	0,008	0,008	0,007	0,007	0,007	0,007	4,761E-05
250, 5s, 1.5cm	0,084	0,078	0,081	0,079	0,081	0,081	0,079	0,080	0,076	0,077	0,080	7,471E-04
210, 5s, 1.5cm	0,074	0,072	0,071	0,068	0,070	0,068	0,068	0,072	0,073	0,072	0,071	6,588E-04
140, 5s, 1.5cm	0,037	0,037	0,036	0,035	0,035	0,037	0,037	0,036	0,036	0,036	0,036	2,097E-04
70, 5s, 1.5cm	0,006	0,007	0,007	0,007	0,007	0,007	0,007	0,007	0,007	0,007	0,007	3,350E-05
250, 5s, 1cm	0,007	0,065	0,065	0,064	0,063	0,063	0,065	0,065	0,063	0,063	0,058	5,708E-03
210, 5s, 1cm	0,060	0,058	0,057	0,058	0,058	0,057	0,056	0,055	0,056	0,059	0,057	4,667E-04
140, 5s, 1cm	0,033	0,033	0,033	0,032	0,035	0,035	0,034	0,034	0,034	0,033	0,034	2,711E-04
70, 5s, 1cm	0,006	0,006	0,006	0,006	0,006	0,006	0,006	0,006	0,006	0,006	0,006	5,783E-05
250, 1.5s, 3cm	0,101	0,100	0,099	0,099	0,099	0,099	0,098	0,101	0,100	0,101	0,100	3,025E-04
210, 1.5s, 3cm	0,090	0,087	0,089	0,090	0,090	0,090	0,089	0,090	0,089	0,089	0,089	3,391E-04
140, 1.5s, 3cm	0,047	0,047	0,046	0,046	0,046	0,046	0,047	0,046	0,047	0,046	0,046	1,439E-04
70, 1.5s, 3cm	0,008	0,008	0,008	0,008	0,008	0,008	0,008	0,008	0,008	0,008	0,008	2,906E-05
250, 1.5s, 1.5cm	0,080	0,078	0,081	0,082	0,081	0,079	0,079	0,079	0,080	0,081	0,080	3,607E-04
210, 1.5s, 1.5cm	0,070	0,071	0,071	0,071	0,072	0,072	0,071	0,072	0,072	0,071	0,071	2,359E-04
140, 1.5s, 1.5cm	0,037	0,037	0,038	0,038	0,037	0,037	0,037	0,037	0,037	0,037	0,037	1,009E-04
70, 1.5s, 1.5cm	0,007	0,007	0,007	0,007	0,007	0,007	0,007	0,007	0,007	0,007	0,007	4,069E-05
250, 1.5s, 1cm	0,068	0,066	0,066	0,066	0,065	0,065	0,066	0,065	0,067	0,066	0,066	2,813E-04
210, 1.5s, 1cm	0,061	0,060	0,059	0,060	0,058	0,058	0,060	0,059	0,060	0,059	0,059	2,919E-04
140, 1.5s, 1cm	0,034	0,035	0,034	0,033	0,035	0,034	0,033	0,034	0,034	0,034	0,034	1,955E-04
70, 1.5s, 1cm	0,006	0,006	0,006	0,006	0,006	0,006	0,006	0,006	0,006	0,006	0,006	4,269E-05
250, 1s, 3cm	0,107	0,104	0,100	0,100	0,101	0,100	0,102	0,100	0,100	0,100	0,101	6,980E-04
210, 1s, 3cm	0,088	0,090	0,089	0,089	0,089	0,089	0,088	0,089	0,087	0,089	0,089	2,441E-04
140, 1s, 3cm	0,046	0,046	0,045	0,046	0,047	0,047	0,046	0,046	0,047	0,047	0,046	2,195E-04
70, 1s, 3cm	0,008	0,008	0,008	0,007	0,007	0,008	0,007	0,007	0,007	0,008	0,007	8,622E-05
250, 1s, 1.5cm	0,082	0,080	0,082	0,081	0,080	0,079	0,080	0,079	0,080	0,081	0,080	3,293E-04
210, 1s, 1.5cm	0,071	0,072	0,071	0,072	0,071	0,072	0,072	0,072	0,071	0,071	0,071	1,318E-04
140, 1s, 1.5cm	0,037	0,036	0,037	0,037	0,037	0,037	0,037	0,037	0,037	0,036	0,037	1,476E-04
70, 1s, 1.5cm	0,007	0,006	0,006	0,007	0,007	0,007	0,006	0,007	0,006	0,007	0,006	5,588E-05
250, 1s, 1cm	0,069	0,067	0,066	0,066	0,065	0,067	0,067	0,067	0,066	0,067	0,067	3,093E-04
210, 1s, 1cm	0,061	0,060	0,059	0,060	0,059	0,058	0,059	0,059	0,059	0,059	0,059	2,711E-04
140, 1s, 1cm	0,035	0,034	0,034	0,035	0,035	0,035	0,035	0,035	0,035	0,035	0,035	1,035E-04
70, 1s, 1cm	0,006	0,006	0,006	0,006	0,006	0,006	0,006	0,006	0,006	0,006	0,006	7,180E-05

Brass nozzle												Average	SEM
250, 10s, 3cm											start	0,000	0,000E+00
Mass (g)	0,043	0,040	0,042	0,037	0,041	0,038	0,040	0,039	0,038	0,038	Mass (g)	0,039	5,993E-04
First Mass at the start of the Stability plateau (g) A	0,041	0,039	0,041	0,037	0,039	0,036	0,039	0,038	0,037	0,038	A	0,038	5,052E-04
Middle Mass at the start of the Stability plateau (g) I	0,041	0,038	0,039	0,035	0,038	0,035	0,038	0,036	0,036	0,036	B	0,037	5,650E-04
Final Mass at the start of the Stability plateau (g) C	0,038	0,035	0,036	0,032	0,035	0,032	0,036	0,035	0,033	0,033	C	0,034	5,749E-04
140, 10s, 3cm											start	0,000	0,000E+00
Mass (g)	0,016	0,016	0,015	0,016	0,015	0,015	0,016	0,016	0,014	0,015	Mass (g)	0,015	1,397E-04
First Mass at the start of the Stability plateau (g) A	0,015	0,015	0,015	0,015	0,015	0,015	0,015	0,015	0,014	0,015	A	0,015	1,306E-04
Middle Mass at the start of the Stability plateau (g) I	0,014	0,014	0,014	0,015	0,015	0,013	0,014	0,014	0,013	0,014	B	0,014	2,422E-04
Final Mass at the start of the Stability plateau (g) C	0,013	0,014	0,014	0,014	0,014	0,013	0,014	0,014	0,013	0,013	C	0,013	1,600E-04
250, 10s, 1.5cm											start	0,000	0,000E+00
Mass (g)	0,037	0,037	0,039	0,036	0,035	0,036	0,034	0,036	0,034	0,034	Mass (g)	0,036	5,271E-04
First Mass at the start of the Stability plateau (g) A	0,037	0,036	0,031	0,036	0,035	0,036	0,033	0,035	0,034	0,033	A	0,035	5,651E-04
Middle Mass at the start of the Stability plateau (g) I	0,035	0,033	0,028	0,034	0,033	0,033	0,032	0,034	0,032	0,032	B	0,033	5,423E-04
Final Mass at the start of the Stability plateau (g) C	0,033	0,032	0,028	0,031	0,032	0,032	0,032	0,032	0,031	0,031	C	0,031	4,457E-04
140, 10s, 1.5cm											start	0,000	0,000E+00
Mass (g)	0,015	0,014	0,014	0,014	0,014	0,014	0,014	0,014	0,015	0,014	Mass (g)	0,014	5,121E-05
First Mass at the start of the Stability plateau (g) A	0,014	0,014	0,014	0,014	0,014	0,014	0,014	0,013	0,014	0,014	A	0,014	5,821E-05
Middle Mass at the start of the Stability plateau (g) I	0,013	0,013	0,012	0,013	0,013	0,013	0,013	0,012	0,013	0,013	B	0,013	9,452E-05
Final Mass at the start of the Stability plateau (g) C	0,013	0,012	0,012	0,013	0,013	0,012	0,013	0,012	0,013	0,013	C	0,013	7,303E-05
250, 10s, 1cm											start	0,000	0,000E+00
Mass (g)	0,038	0,034	0,034	0,033	0,033	0,033	0,033	0,034	0,034	0,033	Mass (g)	0,034	4,387E-04
First Mass at the start of the Stability plateau (g) A	0,037	0,034	0,033	0,033	0,033	0,033	0,032	0,034	0,033	0,032	A	0,033	4,510E-04
Middle Mass at the start of the Stability plateau (g) I	0,036	0,032	0,031	0,031	0,031	0,031	0,030	0,032	0,031	0,031	B	0,032	4,698E-04
Final Mass at the start of the Stability plateau (g) C	0,034	0,031	0,030	0,029	0,030	0,030	0,030	0,029	0,030	0,029	C	0,030	4,403E-04
140, 10s, 1cm											start	0,000	0,000E+00
Mass (g)	0,014	0,014	0,014	0,014	0,015	0,014	0,014	0,014	0,014	0,014	Mass (g)	0,014	6,360E-05
First Mass at the start of the Stability plateau (g) A	0,014	0,014	0,013	0,013	0,014	0,014	0,014	0,014	0,014	0,014	A	0,014	9,165E-05
Middle Mass at the start of the Stability plateau (g) I	0,013	0,013	0,013	0,012	0,013	0,013	0,013	0,013	0,013	0,013	B	0,013	8,825E-05
Final Mass at the start of the Stability plateau (g) C	0,013	0,012	0,012	0,012	0,013	0,012	0,012	0,012	0,012	0,013	C	0,012	1,041E-04
250, 10s, 0.5cm											start	0,000	0,000E+00
Mass (g)	0,035	0,035	0,035	0,032	0,031	0,031	0,030	0,032	0,032	0,031	Mass (g)	0,032	5,556E-04
First Mass at the start of the Stability plateau (g) A	0,035	0,034	0,035	0,032	0,031	0,030	0,030	0,032	0,031	0,030	A	0,032	5,988E-04
Middle Mass at the start of the Stability plateau (g) I	0,032	0,032	0,032	0,029	0,029	0,028	0,028	0,029	0,029	0,028	B	0,030	5,555E-04
Final Mass at the start of the Stability plateau (g) C	0,031	0,030	0,030	0,029	0,028	0,027	0,027	0,027	0,027	0,027	C	0,028	4,610E-04
140, 10s, 0.5cm											start	0,000	0,000E+00
Mass (g)	0,014	0,014	0,014	0,013	0,013	0,014	0,013	0,014	0,014	0,013	Mass (g)	0,014	8,667E-05
First Mass at the start of the Stability plateau (g) A	0,014	0,013	0,013	0,013	0,013	0,013	0,013	0,013	0,013	0,013	A	0,013	1,043E-04
Middle Mass at the start of the Stability plateau (g) I	0,013	0,012	0,013	0,012	0,012	0,012	0,012	0,012	0,012	0,012	B	0,012	8,570E-05
Final Mass at the start of the Stability plateau (g) C	0,012	0,012	0,012	0,012	0,012	0,012	0,012	0,012	0,012	0,012	C	0,012	5,812E-05
250, 5s, 3cm											start	0,000	0,000E+00
Mass (g)	0,040	0,040	0,038	0,040	0,042	0,041	0,040	0,040	0,040	0,041	Mass (g)	0,040	3,538E-04
First Mass at the start of the Stability plateau (g) A	0,039	0,040	0,038	0,039	0,041	0,040	0,040	0,039	0,039	0,041	A	0,040	2,968E-04
Middle Mass at the start of the Stability plateau (g) I	0,038	0,038	0,036	0,037	0,038	0,038	0,038	0,036	0,036	0,039	B	0,037	2,766E-04
Final Mass at the start of the Stability plateau (g) C	0,037	0,038	0,035	0,037	0,037	0,038	0,038	0,037	0,036	0,037	C	0,037	3,236E-04
140, 5s, 3cm											start	0,000	0,000E+00
Mass (g)	0,016	0,016	0,017	0,016	0,016	0,016	0,016	0,016	0,016	0,017	Mass (g)	0,016	9,568E-05
First Mass at the start of the Stability plateau (g) A	0,016	0,016	0,016	0,016	0,016	0,016	0,016	0,015	0,015	0,016	A	0,016	1,055E-04
Middle Mass at the start of the Stability plateau (g) I	0,015	0,016	0,016	0,016	0,016	0,015	0,016	0,015	0,015	0,016	B	0,016	1,713E-04
Final Mass at the start of the Stability plateau (g) C	0,014	0,016	0,016	0,015	0,016	0,014	0,016	0,015	0,015	0,015	C	0,015	2,368E-04
250, 5s, 1.5cm											start	0,000	0,000E+00
Mass (g)	0,039	0,036	0,037	0,036	0,035	0,036	0,036	0,035	0,036	0,036	Mass (g)	0,036	3,459E-04
First Mass at the start of the Stability plateau (g) A	0,039	0,036	0,037	0,036	0,035	0,036	0,036	0,035	0,036	0,036	A	0,036	3,483E-04
Middle Mass at the start of the Stability plateau (g) I	0,038	0,036	0,353	0,036	0,034	0,036	0,035	0,034	0,036	0,035	B	0,067	3,174E-02
Final Mass at the start of the Stability plateau (g) C	0,037	0,034	0,035	0,346	0,328	0,034	0,034	0,033	0,034	0,034	C	0,095	4,039E-02
140, 5s, 1.5cm											start	0,000	0,000E+00
Mass (g)	0,015	0,015	0,015	0,015	0,015	0,015	0,015	0,015	0,015	0,015	Mass (g)	0,015	7,860E-05
First Mass at the start of the Stability plateau (g) A	0,015	0,015	0,015	0,015	0,015	0,015	0,015	0,014	0,014	0,014	A	0,015	1,009E-04
Middle Mass at the start of the Stability plateau (g) I	0,015	0,015	0,014	0,014	0,015	0,014	0,015	0,014	0,014	0,014	B	0,014	1,267E-04
Final Mass at the start of the Stability plateau (g) C	0,014	0,014	0,013	0,014	0,014	0,012	0,014	0,014	0,013	0,014	C	0,014	1,668E-04
250, 5s, 1cm											start	0,000	0,000E+00
Mass (g)	0,038	0,036	0,037	0,035	0,035	0,035	0,036	0,035	0,035	0,034	Mass (g)	0,035	3,489E-04
First Mass at the start of the Stability plateau (g) A	0,038	0,035	0,037	0,034	0,035	0,034	0,035	0,035	0,035	0,034	A	0,035	3,728E-04
Middle Mass at the start of the Stability plateau (g) I	0,036	0,034	0,035	0,033	0,033	0,034	0,034	0,034	0,033	0,033	B	0,034	3,358E-04
Final Mass at the start of the Stability plateau (g) C	0,036	0,034	0,035	0,032	0,032	0,032	0,033	0,033	0,032	0,032	C	0,033	4,144E-04
140, 5s, 1cm											start	0,000	0,000E+00
Mass (g)	0,015	0,015	0,015	0,016	0,015	0,015	0,015	0,015	0,015	0,015	Mass (g)	0,015	1,106E-04
First Mass at the start of the Stability plateau (g) A	0,015	0,014	0,015	0,015	0,015	0,014	0,014	0,014	0,014	0,015	A	0,015	1,164E-04
Middle Mass at the start of the Stability plateau (g) I	0,014	0,014	0,014	0,014	0,014	0,014	0,014	0,014	0,014	0,015	B	0,014	1,062E-04
Final Mass at the start of the Stability plateau (g) C	0,014	0,013	0,013	0,014	0,014	0,013	0,013	0,014	0,013	0,013	C	0,013	1,232E-04
250, 5s, 0.5cm											start	0,000	0,000E+00
Mass (g)	0,035	0,033	0,033	0,033	0,033	0,033	0,034	0,033	0,033	0,033	Mass (g)	0,033	2,308E-04
First Mass at the start of the Stability plateau (g) A	0,035	0,032	0,033	0,033	0,032	0,033	0,033	0,033	0,032	0,033	A	0,033	2,902E-04
Middle Mass at the start of the Stability plateau (g) I	0,033	0,032	0,032	0,032	0,030	0,031	0,031	0,031	0,030	0,031	B	0,031	2,564E-04
Final Mass at the start of the Stability plateau (g) C	0,032	0,030	0,031	0,030	0,030	0,030	0,031	0,030	0,029	0,031	C	0,030	2,802E-04
140, 5s, 0.5cm											start	0,000	0,000E+00
Mass (g)	0,014	0,014	0,014	0,014	0,014	0,014	0,014	0,014	0,014	0,014	Mass (g)	0,014	6,633E-05
First Mass at the start of the Stability plateau (g) A	0,014	0,013	0,013	0,013	0,013	0,013	0,013	0,013	0,014	0,013	A	0,013	4,422E-05
Middle Mass at the start of the Stability plateau (g) I	0,013	0,013	0,013	0,013	0,013	0,013	0,013	0,013	0,013	0,013	B	0,013	4,069E-05
Final Mass at the start of the Stability plateau (g) C	0,013	0,012	0,013	0,013	0,012	0,013	0,013	0,013	0,013	0,013	C	0,013	5,667E-05

Without nozzle												Average	SEM
250, 10s, 3cm											**start**	**0**	0
Mass (g)	0,1036	0,0993	0,0964	0,1006	0,0959	0,0944	0,0932	0,0897	0,0988	0,0935	Mass (g)	0,09654	0,00129634
First Mass at the start of the Stability plateau (g) A	0,103	0,099	0,093	0,1	0,096	0,093	0,092	0,089	0,094	0,0926	A	0,09524	0,00135402
Middle Mass at the start of the Stability plateau (g) B	0,097	0,092	0,089	0,093	0,091	0,089	0,089	0,087	0,089	0,087	B	0,09014	0,00098964
Final Mass at the start of the Stability plateau (g) C	0,093	0,088	0,088	0,088	0,087	0,085	0,086	0,085	0,086	0,0853	C	0,08724	0,00078205
140, 10s, 3cm											**start**	**0**	0
Mass (g)	0,0454	0,0433	0,0437	0,0426	0,0433	0,0428	0,0454	0,0454	0,0438	0,0431	Mass (g)	0,04388	0,00035049
First Mass at the start of the Stability plateau (g) A	0,045	0,043	0,043	0,042	0,042	0,042	0,045	0,045	0,044	0,0423	A	0,04325	0,00040832
Middle Mass at the start of the Stability plateau (g) B	0,043	0,04	0,041	0,041	0,04	0,04	0,043	0,044	0,043	0,0408	B	0,04153	0,00044072
Final Mass at the start of the Stability plateau (g) C	0,041	0,04	0,04	0,039	0,038	0,038	0,042	0,042	0,042	0,0395	C	0,04008	0,0005035
250, 10s, 1.5cm											**start**	**0**	0
Mass (g)	0,0826	0,0749	0,0781	0,0815	0,0794	0,078	0,0806	0,0813	0,0767	0,0816	Mass (g)	0,07947	0,00078656
First Mass at the start of the Stability plateau (g) A	0,081	0,074	0,077	0,081	0,079	0,076	0,078	0,081	0,076	0,0808	A	0,07831	0,00083459
Middle Mass at the start of the Stability plateau (g) B	0,079	0,072	0,071	0,075	0,075	0,071	0,075	0,076	0,073	0,076	B	0,07418	0,00083464
Final Mass at the start of the Stability plateau (g) C	0,075	0,067	0,066	0,073	0,071	0,066	0,068	0,068	0,066	0,054	C	0,06754	0,00181415
140, 10s, 1.5cm											**start**	**0**	0
Mass (g)	0,037	0,0354	0,0369	0,0358	0,0366	0,0376	0,0364	0,0356	0,0353	0,0359	Mass (g)	0,03625	0,00024324
First Mass at the start of the Stability plateau (g) A	0,036	0,034	0,035	0,035	0,036	0,037	0,036	0,035	0,034	0,0353	A	0,03532	0,00027072
Middle Mass at the start of the Stability plateau (g) B	0,034	0,032	0,034	0,032	0,034	0,034	0,034	0,033	0,033	0,0331	B	0,03323	0,00022214
Final Mass at the start of the Stability plateau (g) C	0,032	0,031	0,033	0,031	0,033	0,033	0,032	0,032	0,032	0,0312	C	0,03193	0,00021084
250, 10s, 1cm											**start**	**0**	0
Mass (g)	0,0661	0,0643	0,0624	0,0606	0,0615	0,0628	0,0607	0,0644	0,0623	0,0621	Mass (g)	0,06272	0,00055253
First Mass at the start of the Stability plateau (g) A	0,065	0,063	0,061	0,064	0,058	0,059	0,057	0,063	0,059	0,0605	A	0,06097	0,00087281
Middle Mass at the start of the Stability plateau (g) B	0,063	0,059	0,058	0,055	0,056	0,056	0,056	0,06	0,058	0,0562	B	0,0577	0,0007919
Final Mass at the start of the Stability plateau (g) C	0,06	0,057	0,056	0,056	0,054	0,055	0,044	0,058	0,056	0,0549	C	0,055	0,00131732
140, 10s, 1cm											**start**	**0**	0
Mass (g)	0,034	0,0339	0,033	0,0334	0,0347	0,0334	0,0335	0,0332	0,0329	0,0338	Mass (g)	0,03358	0,00016984
First Mass at the start of the Stability plateau (g) A	0,033	0,032	0,032	0,033	0,034	0,032	0,033	0,032	0,032	0,0312	A	0,03243	0,00025036
Middle Mass at the start of the Stability plateau (g) B	0,032	0,031	0,03	0,03	0,032	0,031	0,031	0,03	0,03	0,0295	B	0,0307	0,00026499
Final Mass at the start of the Stability plateau (g) C	0,03	0,03	0,03	0,029	0,031	0,03	0,03	0,03	0,029	0,0291	C	0,02965	0,00016482
250, 5s, 3cm											**start**	**0**	0
Mass (g)	0,1036	0,0963	0,0961	0,0936	0,0925	0,0997	0,1002	0,0984	0,0956	0,0962	Mass (g)	0,09722	0,00104497
First Mass at the start of the Stability plateau (g) A	0,104	0,096	0,096	0,093	0,092	0,1	0,1	0,097	0,094	0,0941	A	0,0965	0,00114358
Middle Mass at the start of the Stability plateau (g) B	0,101	0,093	0,092	0,091	0,091	0,095	0,094	0,093	0,092	0,0917	B	0,09332	0,0009259
Final Mass at the start of the Stability plateau (g) C	0,1	0,092	0,09	0,09	0,089	0,093	0,092	0,091	0,089	0,0901	C	0,09163	0,00097275
140, 5s, 3cm											**start**	**0**	0
Mass (g)	0,0455	0,0446	0,0425	0,0444	0,0472	0,0463	0,0458	0,0455	0,0443	0,0453	Mass (g)	0,04514	0,00040585
First Mass at the start of the Stability plateau (g) A	0,045	0,044	0,042	0,044	0,047	0,045	0,045	0,044	0,044	0,0451	A	0,04445	0,00040586
Middle Mass at the start of the Stability plateau (g) B	0,043	0,041	0,041	0,041	0,045	0,043	0,044	0,043	0,044	0,0444	B	0,04289	0,00046677
Final Mass at the start of the Stability plateau (g) C	0,041	0,041	0,041	0,04	0,444	0,042	0,043	0,043	0,044	0,0439	C	0,08224	0,04019799
250, 5s, 1.5cm											**start**	**0**	0
Mass (g)	0,084	0,0781	0,0812	0,079	0,0812	0,0811	0,0793	0,0795	0,076	0,0768	Mass (g)	0,07962	0,00074711
First Mass at the start of the Stability plateau (g) A	0,083	0,077	0,078	0,078	0,081	0,08	0,079	0,079	0,075	0,0753	A	0,07851	0,00076295
Middle Mass at the start of the Stability plateau (g) B	0,08	0,075	0,008	0,077	0,077	0,077	0,076	0,076	0,072	0,0735	B	0,06904	0,00685135
Final Mass at the start of the Stability plateau (g) C	0,08	0,075	0,008	0,075	0,074	0,075	0,074	0,073	0,071	0,0733	C	0,06794	0,00673267
140, 5s, 1.5cm											**start**	**0**	0
Mass (g)	0,0366	0,0368	0,0363	0,0354	0,0354	0,0374	0,0368	0,0364	0,0361	0,0356	Mass (g)	0,03628	0,00020966
First Mass at the start of the Stability plateau (g) A	0,036	0,036	0,035	0,035	0,035	0,037	0,036	0,036	0,036	0,0348	A	0,03546	0,00022862
Middle Mass at the start of the Stability plateau (g) B	0,034	0,034	0,033	0,033	0,033	0,035	0,034	0,034	0,034	0,0332	B	0,03366	0,00019505
Final Mass at the start of the Stability plateau (g) C	0,033	0,033	0,033	0,033	0,033	0,035	0,034	0,033	0,033	0,0331	C	0,03319	0,00017349
250, 5s, 1cm											**start**	**0**	0
Mass (g)	0,0069	0,0652	0,0648	0,0635	0,0631	0,0628	0,0653	0,0645	0,0631	0,0632	Mass (g)	0,058244	0,00570818
First Mass at the start of the Stability plateau (g) A	0,066	0,064	0,063	0,062	0,062	0,06	0,061	0,063	0,062	0,0616	A	0,06247	0,00047189
Middle Mass at the start of the Stability plateau (g) B	0,065	0,061	0,06	0,06	0,06	0,059	0,058	0,06	0,058	0,0584	B	0,05981	0,0006806
Final Mass at the start of the Stability plateau (g) C	0,063	0,06	0,058	0,058	0,058	0,057	0,058	0,059	0,057	0,0574	C	0,05842	0,00056071
140, 5s, 1cm											**start**	**0**	0
Mass (g)	0,0334	0,0334	0,0329	0,0323	0,0349	0,0347	0,0344	0,0343	0,0343	0,0332	Mass (g)	0,03378	0,00027113
First Mass at the start of the Stability plateau (g) A	0,033	0,032	0,032	0,032	0,034	0,034	0,034	0,033	0,034	0,0329	A	0,0329	0,00025122
Middle Mass at the start of the Stability plateau (g) B	0,032	0,031	0,031	0,031	0,032	0,032	0,032	0,031	0,032	0,0313	B	0,03142	0,00013646
Final Mass at the start of the Stability plateau (g) C	0,032	0,031	0,03	0,03	0,032	0,031	0,032	0,023	0,03	0,031	C	0,03016	0,00082707

8.2. Annex 2

No Nozzle 1,5s								
Vertical diameter	**250**	**SEM**	**210**	**SEM**	**140**	**SEM**	**70**	**SEM**
3 cm	1,381	0,034	1,241	0,019				
1,5 cm	1,488	0,012	1,523	0,000	0,875	0,009	0,875	
1 cm	1,680	0,057	1,549	0,125	1,228	0,264	0,955	
0,5 cm	1,820	0,059	1,720	0,006	1,195	0,003	1,198	
Horizontal diameter	**250**	**SEM**	**210**	**SEM**	**140**	**SEM**	**70**	**SEM**
3 cm	1,384	0,006	1,253	0,012				
1,5 cm	1,529	0,003	1,586	0,012	0,908	0,033		
1 cm	1,767	0,022	1,592	0,127	0,978	0,022		
0,5 cm	1,914	0,032	1,732	0,044	1,209	0,012	0,234	
Nozzle 1,5s								
Vertical diameter	**250**	**SEM**	**210**	**SEM**	**140**	**SEM**	**70**	**SEM**
3 cm	1,168	0,055	1,060	0,013	0,764	0,088		
1,5 cm	0,825	0,249	1,045	0,003	0,913	0,006	0,388	0,026
1 cm	1,202	0,046	1,130	0,020	0,874	0,033	0,365	0,148
0,5 cm	1,248	0,023	1,112	0,088	0,950	0,036	0,415	0,006
Horizontal diameter	**250**	**SEM**	**210**	**SEM**	**140**	**SEM**	**70**	**SEM**
3 cm	1,197	0,065	1,092	0,007	0,739	0,033		
1,5 cm	1,128	0,042	1,087	0,006	0,914	0,064	0,371	0,038
1 cm	1,236	0,052	1,174	0,023	0,902	0,007	0,405	0,124
0,5 cm	1,316	0,055	1,274	0,019	0,981	0,032	0,423	0,000
No Nozzle 0,9s								
Vertical diameter	**250**	**SEM**	**210**	**SEM**	**140**	**SEM**	**70**	**SEM**
3 cm	1,047	0,161	1,219	0,084				
1,5 cm	1,473	0,060	1,416	0,048	0,821	0,038	0,886	
1 cm	1,765	0,088	1,622	0,021	0,960	0,058	0,824	
0,5 cm	1,709	0,079	1,737	0,063	0,878	0,022	0,920	
Horizontal diameter	**250**	**SEM**	**210**	**SEM**	**140**	**SEM**	**70**	**SEM**
3 cm	1,119	0,040	1,215	0,036				
1,5 cm	1,484	0,028	1,537	0,032	0,841	0,045		
1 cm	1,773	0,124	1,593	0,029	0,929	0,105		
0,5 cm	1,778	0,038	1,659	0,031	0,970	0,050		
Nozzle 0,9s								
Vertical diameter	**250**	**SEM**	**210**	**SEM**	**140**	**SEM**	**70**	**SEM**
3 cm	1,054	0,052	0,926	0,036				
1,5 cm	1,098	0,009	1,082	0,019	0,826	0,065	0,436	0,034
1 cm	1,253	0,046	3,145	2,023	0,894	0,007	0,388	0,069
0,5 cm	1,417	0,045	1,320	0,057	0,951	0,018	0,409	0,126
Horizontal diameter	**250**	**SEM**	**210**	**SEM**	**140**	**SEM**	**70**	**SEM**
3 cm	1,125	0,078	0,936	0,019	0,000	0,000		
1,5 cm	1,146	0,012	1,133	0,012	0,856	0,053	0,426	0,047
1 cm	1,275	0,072	1,226	0,042	0,894	0,003	0,397	0,085
0,5 cm	1,474	0,040	1,392	0,097	0,970	0,033	0,429	0,131

8.3. Annex 3

Brass Nozzle	Baseline temp.	SEM	SD	Temp. range	SEM	SD	Diam. of 0.1ºC gradient	SEM	SD	Diam. of 0.5ºC gradient	SEM	SD	Diam. of 1.0ºC gradient	SEM	SD
250, 1sec, 3cm	29,433	0,267	0,462	1,733	0,067	0,115	3,345	0,225	0,390	6,464	0,193	0,334	8,940	0,232	0,402
210, 1sec, 3cm	29,800	0,153	0,265	1,700	0,058	0,100	1,512	0,499	0,865	6,464	0,201	0,348	8,554	0,129	0,223
140, 1sec, 3cm	29,900	0,058	0,100	1,667	0,033	0,058	2,219	0,754	1,305	6,175	0,675	1,170	8,908	0,505	0,875
70, 1sec, 3cm	29,900	0,058	0,100	1,767	0,033	0,058	2,219	0,365	0,633	4,953	0,716	1,241	8,490	0,675	1,170
250, 1sec, 1.5cm	29,767	0,088	0,153	2,400	0,000	0,000	1,093	0,196	0,339	3,731	0,161	0,279	5,789	0,096	0,167
210, 1sec, 1.5cm	29,733	0,033	0,058	2,267	0,033	0,058	1,801	0,225	0,390	3,795	0,032	0,056	5,757	0,116	0,201
140, 1sec, 1.5cm	29,700	0,058	0,100	2,300	0,058	0,100	1,126	0,257	0,446	3,859	0,147	0,255	5,789	0,193	0,334
70, 1sec, 1.5cm	29,867	0,033	0,058	2,033	0,067	0,115	0,547	0,179	0,310	1,640	0,056	0,096	2,766	0,085	0,147
250, 1sec, 1cm	30,500	0,058	0,100	2,800	0,000	0,000	0,868	0,147	0,255	2,155	0,064	0,111	3,602	0,085	0,147
210, 1sec, 1cm	30,467	0,033	0,058	2,667	0,033	0,058	0,804	0,116	0,201	2,219	0,056	0,096	3,538	0,032	0,056
140, 1sec, 1cm	30,633	0,033	0,058	2,833	0,033	0,058	0,675	0,096	0,167	1,769	0,032	0,056	3,409	0,032	0,056
70, 1sec, 1cm	30,333	0,133	0,231	2,633	0,088	0,153	0,193	0,056	0,096	0,900	0,032	0,056	1,576	0,116	0,201
250, 1sec, 0.5cm	30,933	0,033	0,058	3,100	0,058	0,100	0,354	0,161	0,279	1,447	0,056	0,096	2,444	0,129	0,223
210, 1sec, 0.5cm	30,600	0,115	0,200	3,000	0,058	0,100	0,772	0,147	0,255	1,704	0,032	0,056	2,830	0,140	0,243
140, 1sec, 0.5cm	30,467	0,033	0,058	2,867	0,067	0,115	0,611	0,085	0,147	1,415	0,032	0,056	2,315	0,096	0,167
70, 1sec, 0.5cm	30,700	0,058	0,100	2,833	0,338	0,586	0,482	0,000	0,000	1,029	0,032	0,056	1,544	0,056	0,096
250, 1.5sec, 1cm	30,033	0,120	0,208	2,900	0,058	0,100	0,515	0,032	0,056	2,219	0,201	0,348	3,698	0,085	0,147
210, 1.5sec, 1cm	29,833	0,120	0,208	2,667	0,067	0,115	0,579	0,096	0,167	2,123	0,147	0,255	3,731	0,161	0,279
140, 1.5sec, 1cm	29,700	0,058	0,100	2,767	0,033	0,058	0,386	0,096	0,167	1,833	0,193	0,334	3,505	0,161	0,279
70, 1.5sec, 1cm	29,733	0,033	0,058	2,533	0,219	0,379	0,289	0,096	0,167	0,933	0,064	0,111	1,608	0,032	0,056
250, 0.5sec, 1cm	30,200	0,000	0,000	2,467	0,088	0,153	0,740	0,275	0,476	2,605	0,193	0,334	3,923	0,129	0,223
210, 0.5sec, 1cm	30,133	0,033	0,058	2,500	0,100	0,173	0,482	0,096	0,167	2,219	0,111	0,193	3,763	0,201	0,348
140, 0.5sec, 1cm	30,133	0,033	0,058	2,600	0,058	0,100	0,547	0,032	0,056	1,930	0,147	0,255	3,763	0,201	0,348
70, 0.5sec, 1cm	30,200	0,058	0,100	1,933	0,120	0,208	0,354	0,140	0,243	1,061	0,056	0,096	2,090	0,225	0,390

No Nozzle	Baseline temp.	SEM	SD	Temp. range	SEM	SD	Diam. of 0.1ºC gradient	SEM	SD	Diam. of 0.5ºC gradient	SEM	SD	Diam. of 1.0ºC gradient	SEM	SD
250, 1sec, 3cm	30,233	0,088	0,153	2,167	0,033	0,058	1,962	0,211	0,365	6,689	0,032	0,056	10,484	0,032	0,056
210, 1sec, 3cm	30,000	0,058	0,100	2,133	0,033	0,058	1,801	0,225	0,390	6,561	0,243	0,421	10,452	0,116	0,201
140, 1sec, 3cm	30,000	0,208	0,361	2,033	0,033	0,058	1,930	0,435	0,754	6,946	0,193	0,334	10,677	0,032	0,056
70, 1sec, 3cm	30,400	0,000	0,000	1,933	0,033	0,058	1,319	0,614	1,063	8,362	0,371	0,642	10,452	0,032	0,056
250, 1sec, 1.5cm	30,567	0,067	0,115	2,400	0,000	0,000	1,897	0,307	0,531	4,920	0,255	0,442	7,815	0,295	0,511
210, 1sec, 1.5cm	30,300	0,058	0,100	2,333	0,033	0,058	1,962	0,161	0,279	5,338	0,032	0,056	8,201	0,111	0,193
140, 1sec, 1.5cm	30,200	0,058	0,100	2,333	0,067	0,115	1,962	0,085	0,147	5,113	0,147	0,255	8,522	0,116	0,201
70, 1sec, 1.5cm	30,300	0,000	0,000	2,000	0,000	0,000	2,476	0,161	0,279	6,689	0,129	0,223	9,937	0,000	0,000
250, 1sec, 1cm	30,267	0,033	0,058	1,867	0,133	0,231	1,222	0,354	0,613	4,406	0,196	0,339	6,754	0,096	0,167
210, 1sec, 1cm	30,167	0,067	0,115	1,533	0,033	0,058	1,351	0,386	0,668	4,277	0,032	0,056	6,850	0,096	0,167
140, 1sec, 1cm	30,233	0,033	0,058	1,467	0,033	0,058	1,351	0,279	0,482	4,760	0,032	0,056	7,976	0,464	0,803
70, 1sec, 1cm	30,233	0,033	0,058	1,333	0,033	0,058	1,286	0,225	0,390	5,178	0,280	0,486	8,683	0,147	0,255
250, 1sec, 0.5cm	31,500	0,058	0,100	1,633	0,067	0,115	2,123	0,966	1,674	6,593	0,085	0,147	8,683	0,255	0,442
210, 1sec, 0.5cm	31,167	0,033	0,058	1,800	0,000	0,000	2,669	1,326	2,296	6,689	0,474	0,821	8,876	0,255	0,442
140, 1sec, 0.5cm	31,067	0,088	0,153	1,633	0,033	0,058	3,152	0,358	0,620	6,561	0,056	0,096	9,069	0,056	0,096
70, 1sec, 0.5cm	31,400	0,058	0,100	1,533	0,033	0,058	2,251	1,227	2,125	7,718	0,386	0,668	10,066	0,064	0,111
250, 1.5sec, 1cm	30,300	0,115	0,200	1,633	0,088	0,153	1,512	0,129	0,223	4,695	0,232	0,402	6,786	0,263	0,456
210, 1.5sec, 1cm	30,233	0,033	0,058	1,467	0,033	0,058	1,286	0,371	0,642	4,663	0,196	0,339	6,432	0,140	0,243
140, 1.5sec, 1cm	30,200	0,000	0,000	1,567	0,033	0,058	0,997	0,064	0,111	4,727	0,147	0,255	6,850	0,096	0,167
70, 1.5sec, 1cm	30,233	0,033	0,058	1,367	0,067	0,115	1,158	0,201	0,348	5,371	0,129	0,223	8,362	0,064	0,111
250, 0.5sec, 1cm	30,467	0,033	0,058	1,300	0,000	0,000	2,315	0,310	0,537	5,306	0,096	0,167	8,136	0,225	0,390
210, 0.5sec, 1cm	30,433	0,033	0,058	1,367	0,033	0,058	1,415	0,161	0,279	5,049	0,140	0,243	8,201	0,255	0,442
140, 0.5sec, 1cm	30,467	0,033	0,058	1,367	0,033	0,058	1,994	0,371	0,642	5,435	0,280	0,486	8,522	0,170	0,295
70, 0.5sec, 1cm	30,533	0,033	0,058	1,167	0,033	0,058	1,576	0,864	1,496	6,496	0,140	0,243	9,133	0,032	0,056

Guide for Authors

Contact Lens & Anterior Eye (The Journal of the British Contact Lens Association) welcomes original contributions pertaining to contact lens theory and practice, as well as those relating to the structure and function of the anterior eye. The Editor-in-Chief does not consider material which has been previously published elsewhere. All manuscripts should be accompanied by a clear statement that the work has not been published elsewhere and is not under review with another journal. All manuscripts are normally evaluated for suitability of publication in the journal by the Editor-in-Chief and two referees.

Types of paper

The journal publishes the following: Full Length Papers, Review Articles, Case Reports, Short Communications, and Correspondence (such as commentary on a published paper or a letter to the editor).

The article should be arranged as follows, where possible: (1) title page including title and author(s), (2) abstract (for Full Length Papers and Review Articles only), (3) key words, (4) text, with figures and tables embedded in the appropriate place, (5) references.

Correspondence does not require to be formatted as this nor will require an abstract. Case reports will only be considered if they are truly novel. Papers that describe a new surgical technique are likely to be rejected, as they will not be of sufficient interest to the majority of the readership. If you are unsure if your paper fits the remit of CLAE then please email the Editor-in-Chief for advice before submission.

Authors are discouraged from the use of personal pronouns in the course of their writing and the preferred writing style is 'third person' style.

Contact details

Suggestions for review article topics or special issues can still be sent to:

Dr Shehzad A. Naroo
Editor-in-Chief, Contact Lens & Anterior Eye
Opthalmic Research Group
School of Life and Health Sciences
Aston University
Birmingham
UK
s.a.naroo@aston.ac.uk

Contact details for questions arising after acceptance of an article, especially those relating to proofs, are provided when an article is accepted for publication.

Submission checklist

You can use this list to carry out a final check of your submission before you send it to the journal for review. Please check the relevant section in this Guide for Authors for more details.

Ensure that the following items are present:

One author has been designated as the corresponding author with contact details:
• E-mail address
• Full postal address

All necessary files have been uploaded:
Manuscript:
• Include keywords
• All figures (include relevant captions)
• All tables (including titles, description, footnotes)
• Ensure all figure and table citations in the text match the files provided
• Indicate clearly if color should be used for any figures in print
Graphical Abstracts / Highlights files (where applicable)
Supplemental files (where applicable)

Further considerations
• Manuscript has been 'spell checked' and 'grammar checked'
• All references mentioned in the Reference List are cited in the text, and vice versa
• Permission has been obtained for use of copyrighted material from other sources (including the Internet)
• A competing interests statement is provided, even if the authors have no competing interests to declare
• Journal policies detailed in this guide have been reviewed
• Referee suggestions and contact details provided, based on journal requirements

For further information, visit our Support Center.

Figures and Tables

Figures and tables should be embedded within the manuscript file at the appropriate point in the manuscript. They should be editable and not embedded as images. Any figure that cannot be embedded within the source file needs to be uploaded separately.

Before You Begin

Ethics in publishing

Please see our information pages on Ethics in publishing and Ethical guidelines for journal publication.

Studies in humans and animals

If the work involves the use of human subjects, the author should ensure that the work described has been carried out in accordance with The Code of Ethics of the World Medical Association (Declaration of Helsinki) for experiments involving humans. The manuscript should be in line with the Recommendations for the Conduct, Reporting, Editing and Publication of Scholarly Work in Medical Journals and aim for the inclusion of representative human populations (sex, age and ethnicity) as per those recommendations. The terms sex and gender should be used correctly.

Authors should include a statement in the manuscript that informed consent was obtained for experimentation with human subjects. The privacy rights of human subjects must always be observed.

All animal experiments should comply with the ARRIVE guidelines and should be carried out in accordance with the U.K. Animals (Scientific Procedures) Act, 1986 and associated guidelines, EU Directive 2010/63/EU for animal experiments, or the National Institutes of Health guide for the care and use of Laboratory animals (NIH Publications No. 8023, revised 1978) and the authors should clearly indicate in the manuscript that such guidelines have been followed. The sex of animals must be indicated, and where appropriate, the influence (or association) of sex on the results of the study.

In case studies the authors should state that they have obtained permission from the subjects to use images for publication. Furthermore, identity of patients should not be revealed.

Declaration of interest

All authors must disclose any financial and personal relationships with other people or organizations that could inappropriately influence (bias) their work. Examples of potential competing interests include employment, consultancies, stock ownership, honoraria, paid expert testimony, patent applications/registrations, and grants or other funding. Authors must disclose any interests in two places: 1. A summary declaration of interest statement in the title page file (if double-blind) or the manuscript file (if single-blind). If there are no interests to declare then please state this: 'Declarations of interest: none'. This summary statement will be ultimately published if the article is accepted. 2. Detailed disclosures as part of a separate Declaration of Interest form, which forms part of the journal's official records. It is important for potential interests to be declared in both places and that the information matches. More information.

Submission declaration and verification

Submission of an article implies that the work described has not been published previously (except in the form of an abstract, a published lecture or academic thesis, see 'Multiple, redundant or concurrent publication' for more information), that it is not under consideration for publication elsewhere, that its publication is approved by all authors and tacitly or explicitly by the responsible authorities where the work was carried out, and that, if accepted, it will not be published elsewhere in the same form, in English or in any other language, including electronically without the written consent of the copyright-holder. To verify originality, your article may be checked by the originality detection service Crossref Similarity Check.

Use of inclusive language

Inclusive language acknowledges diversity, conveys respect to all people, is sensitive to differences, and promotes equal opportunities. Articles should make no assumptions about the beliefs or commitments of any reader, should contain nothing which might imply that one individual is superior to another on the grounds of race, sex, culture or any other characteristic, and should use inclusive language throughout. Authors should ensure that writing is free from bias, for instance by using 'he or she', 'his/her' instead of 'he' or 'his', and by making use of job titles that are free of stereotyping (e.g. 'chairperson' instead of 'chairman' and 'flight attendant' instead of 'stewardess').

Changes to authorship

Authors are expected to consider carefully the list and order of authors **before** submitting their manuscript and provide the definitive list of authors at the time of the original submission. Any addition, deletion or rearrangement of author names in the authorship list should be made only **before** the manuscript has been accepted and only if approved by the journal Editor. To request such a change, the Editor must receive the following from the **corresponding author**: (a) the reason for the change in author list and (b) written confirmation (e-mail, letter) from all authors that they agree with the addition, removal or rearrangement. In the case of addition or removal of authors, this includes confirmation from the author being added or removed.
Only in exceptional circumstances will the Editor consider the addition, deletion or rearrangement of authors **after** the manuscript has been accepted. While the Editor considers the request, publication of the manuscript will be suspended. If the manuscript has already been published in an online issue, any requests approved by the Editor will result in a corrigendum.

Copyright

Upon acceptance of an article, authors will be asked to complete a 'Journal Publishing Agreement' (see more information on this). An e-mail will be sent to the corresponding author confirming receipt of the manuscript together with a 'Journal Publishing Agreement' form or a link to the online version of this agreement.

Subscribers may reproduce tables of contents or prepare lists of articles including abstracts for internal circulation within their institutions. Permission of the Publisher is required for resale or distribution outside the institution and for all other derivative works, including compilations and translations. If excerpts from other copyrighted works are included, the author(s) must obtain written permission from the copyright owners and credit the source(s) in the article. Elsevier has preprinted forms for use by authors in these cases.

For gold open access articles: Upon acceptance of an article, authors will be asked to complete an 'Exclusive License Agreement' (more information). Permitted third party reuse of gold open access articles is determined by the author's choice of user license.

Author rights

As an author you (or your employer or institution) have certain rights to reuse your work. More information.

Elsevier supports responsible sharing
Find out how you can share your research published in Elsevier journals.

Role of the funding source

You are requested to identify who provided financial support for the conduct of the research and/or preparation of the article and to briefly describe the role of the sponsor(s), if any, in study design; in the collection, analysis and interpretation of data; in the writing of the report; and in the decision to submit the article for publication. If the funding source(s) had no such involvement then this should be stated.

Open access

Please visit our Open Access page from the Journal Homepage for more information.

Language (usage and editing services)
Please write your text in good English (American or British usage is accepted, but not a mixture of these). Authors who feel their English language manuscript may require editing to eliminate possible grammatical or spelling errors and to conform to correct scientific English may wish to use the English Language Editing service available from Elsevier's Author Services.

Submission

Our online submission system guides you stepwise through the process of entering your article details and uploading your files. The system converts your article files to a single PDF file used in the peer-review process. Editable files (e.g., Word, LaTeX) are required to typeset your article for final publication. All correspondence, including notification of the Editor's decision and requests for revision, is sent by e-mail.

Submit your article
Please submit your article via https://www.editorialmanager.com/clae/default.aspx.

Preparation

Peer review

This journal operates a double blind review process. All contributions will be initially assessed by the editor for suitability for the journal. Papers deemed suitable are then typically sent to a minimum of one independent expert reviewer to assess the scientific quality of the paper. The Editor is responsible for the final decision regarding acceptance or rejection of articles. The Editor's decision is final. More information on types of peer review.

Double-blind review

This journal uses double-blind review, which means the identities of the authors are concealed from the reviewers, and vice versa. More information is available on our website. To facilitate this, please include the following separately:

Title page (with author details): This should include the title, authors' names, affiliations, acknowledgements and any Declaration of Interest statement, and a complete address for the corresponding author including an e-mail address.
Blinded manuscript (no author details): The main body of the paper (including the references, figures, tables and any acknowledgements) should not include any identifying information, such as the authors' names or affiliations.

Article structure

Essential title page information

• ***Title.*** Concise and informative. Titles are often used in information-retrieval systems. Avoid abbreviations and formulae where possible.
• ***Author names and affiliations.*** Please clearly indicate the given name(s) and family name(s) of each author and check that all names are accurately spelled. You can add your name between parentheses in your own script behind the English transliteration. Present the authors' affiliation addresses (where the actual work was done) below the names. Indicate all affiliations with a lower-case superscript letter immediately after the author's name and in front of the appropriate address. Provide the full postal address of each affiliation, including the country name and, if available, the e-mail address of each author.
• ***Corresponding author.*** Clearly indicate who will handle correspondence at all stages of refereeing and publication, also post-publication. This responsibility includes answering any future queries about Methodology and Materials. **Ensure that the e-mail address is given and that contact details are kept up to date by the corresponding author.**
• ***Present/permanent address.*** If an author has moved since the work described in the article was done, or was visiting at the time, a 'Present address' (or 'Permanent address') may be indicated as a footnote to that author's name. The address at which the author actually did the work must be retained as the main, affiliation address. Superscript Arabic numerals are used for such footnotes.

Abstract

A concise and factual abstract is required. The abstract should state briefly the purpose of the research, the principal results and major conclusions. An abstract is often presented separately from the article, so it must be able to stand alone. For this reason, References should be avoided, but if essential, then cite the author(s) and year(s). Also, non-standard or uncommon abbreviations should be avoided, but if essential they must be defined at their first mention in the abstract itself.

Graphical abstract

Although a graphical abstract is optional, its use is encouraged as it draws more attention to the online article. The graphical abstract should summarize the contents of the article in a concise, pictorial form designed to capture the attention of a wide readership. Graphical abstracts should be submitted as a separate file in the online submission system. Image size: Please provide an image with a minimum of 531 × 1328 pixels (h × w) or proportionally more. The image should be readable at a size of 5 × 13 cm using a regular screen resolution of 96 dpi. Preferred file types: TIFF, EPS, PDF or MS Office files. You can view Example Graphical Abstracts on our information site.

Authors can make use of Elsevier's Illustration Services to ensure the best presentation of their images and in accordance with all technical requirements.

Keywords

Three to six key words should appear below the abstract to assist in indexing.

Formatting of funding sources
List funding sources in this standard way to facilitate compliance to funder's requirements:

Funding: This work was supported by the National Institutes of Health [grant numbers xxxx, yyyy]; the Bill & Melinda Gates Foundation, Seattle, WA [grant number zzzz]; and the United States Institutes of Peace [grant number aaaa].

It is not necessary to include detailed descriptions on the program or type of grants and awards. When funding is from a block grant or other resources available to a university, college, or other research institution, submit the name of the institute or organization that provided the funding.

If no funding has been provided for the research, please include the following sentence:

This research did not receive any specific grant from funding agencies in the public, commercial, or not-for-profit sectors.

Page and line numbering

Pages and lines should be numbered prior to submission. Line numbers should start on the first page, be continuous and not restarted on each page.

Artwork

Electronic artwork
General points
• Make sure you use uniform lettering and sizing of your original artwork.
• Embed the used fonts if the application provides that option.
• Aim to use the following fonts in your illustrations: Arial, Courier, Times New Roman, Symbol, or use fonts that look similar.
• Number the illustrations according to their sequence in the text.
• Use a logical naming convention for your artwork files.
• Provide captions to illustrations separately.
• Size the illustrations close to the desired dimensions of the published version.
• Submit each illustration as a separate file.
• Ensure that color images are accessible to all, including those with impaired color vision.

A detailed guide on electronic artwork is available.
You are urged to visit this site; some excerpts from the detailed information are given here.
Formats
If your electronic artwork is created in a Microsoft Office application (Word, PowerPoint,

Excel) then please supply 'as is' in the native document format.
Regardless of the application used other than Microsoft Office, when your electronic artwork is finalized, please 'Save as' or convert the images to one of the following formats (note the resolution requirements for line drawings, halftones, and line/halftone combinations given below):
EPS (or PDF): Vector drawings, embed all used fonts.
TIFF (or JPEG): Color or grayscale photographs (halftones), keep to a minimum of 300 dpi.
TIFF (or JPEG): Bitmapped (pure black & white pixels) line drawings, keep to a minimum of 1000 dpi.
TIFF (or JPEG): Combinations bitmapped line/half-tone (color or grayscale), keep to a minimum of 500 dpi.
Please do not:
• Supply files that are optimized for screen use (e.g., GIF, BMP, PICT, WPG); these typically have a low number of pixels and limited set of colors;
• Supply files that are too low in resolution;
• Submit graphics that are disproportionately large for the content.

Color artwork
Please make sure that artwork files are in an acceptable format (TIFF (or JPEG), EPS (or PDF) or MS Office files) and with the correct resolution. If, together with your accepted article, you submit usable color figures then Elsevier will ensure, at no additional charge, that these figures will appear in color online (e.g., ScienceDirect and other sites) in addition to color reproduction in print. Further information on the preparation of electronic artwork.

Line drawings
All lettering, graph lines and points on graphs should be sufficiently large and bold to permit reproduction when the diagram has been reduced to a size suitable for inclusion in the journal. Do not use any type of shading on computer-generated illustrations.

Photographs
Original photographs must be supplied as they are to be reproduced (e.g. black and white or colour). If necessary, a scale should be marked on the photograph. These can be supplied as hard copy to follow an online article submission if necessary.

Figure captions
Ensure that each illustration has a caption. Supply captions separately, not attached to the figure. A caption should comprise a brief title (**not** on the figure itself) and a description of the illustration. Keep text in the illustrations themselves to a minimum but explain all symbols and abbreviations used.

Tables

Each table should be intelligible without reference to the text. Tables should be numbered with Arabic numerals in the order they are referred to the in the text. Footnotes to tables should be given below the table and should be referred to by superscript lowercase letters. No vertical rules should be used. Tables should not duplicate results presented elsewhere in the manuscript (e.g. in graphs).

Citation in text

Please ensure that every reference cited in the text is also present in the reference list (and vice versa). Any references cited in the abstract must be given in full. Unpublished results and personal communications are not recommended in the reference list, but may be mentioned in the text. If these references are included in the reference list they should follow the standard reference style of the journal and should include a substitution of the publication date with either 'Unpublished results' or 'Personal communication'. Citation of a reference as 'in press' implies that the item has been accepted for publication.

Data references

This journal encourages you to cite underlying or relevant datasets in your manuscript by citing them in your text and including a data reference in your Reference List. Data references should include the following elements: author name(s), dataset title, data repository, version (where available), year, and global persistent identifier. Add [dataset] immediately before the reference so we can properly identify it as a data reference. The [dataset] identifier will not appear in your published article.

Reference management software

Most Elsevier journals have their reference template available in many of the most popular reference management software products. These include all products that support Citation Style Language styles, such as Mendeley. Using citation plug-ins from these products, authors only need to select the appropriate journal template when preparing their article, after which citations and bibliographies will be automatically formatted in the journal's style. If no template is yet available for this journal, please follow the format of the sample references and citations as shown in this Guide. If you use reference management software, please ensure that you remove all field codes before submitting the electronic manuscript. More information on how to remove field codes from different reference management software.

Users of Mendeley Desktop can easily install the reference style for this journal by clicking the following link:
http://open.mendeley.com/use-citation-style/contact-lens-and-anterior-eye
When preparing your manuscript, you will then be able to select this style using the Mendeley plug-ins for Microsoft Word or LibreOffice.

Reference style

Text: Indicate references by number(s) in square brackets in line with the text. The actual authors can be referred to, but the reference number(s) must always be given.
List: Number the references (numbers in square brackets) in the list in the order in which they appear in the text.
Examples:
Reference to a journal publication:
[1] Van der Geer J, Hanraads JAJ, Lupton RA. The art of writing a scientific article. J Sci Commun 2010;163:51–9. https://doi.org/10.1016/j.Sc.2010.00372.
Reference to a journal publication with an article number:
[2] Van der Geer J, Hanraads JAJ, Lupton RA. The art of writing a scientific article. Heliyon. 2018;19:e00205. https://doi.org/10.1016/j.heliyon.2018.e00205
Reference to a book:
[3] Strunk Jr W, White EB. The elements of style. 4th ed. New York: Longman; 2000.
Reference to a chapter in an edited book:

[4] Mettam GR, Adams LB. How to prepare an electronic version of your article. In: Jones BS, Smith RZ, editors. Introduction to the electronic age, New York: E-Publishing Inc; 2009, p. 281–304.
Reference to a website:
[5] Cancer Research UK. Cancer statistics reports for the UK, http://www.cancerresearchuk.org/aboutcancer/statistics/cancerstatsreport/; 2003 [accessed 13 March 2003].
Reference to a dataset:
[dataset] [6] Oguro M, Imahiro S, Saito S, Nakashizuka T. Mortality data for Japanese oak wilt disease and surrounding forest compositions, Mendeley Data, v1; 2015. https://doi.org/10.17632/xwj98nb39r.1.
Note shortened form for last page number. e.g., 51–9, and that for more than 6 authors the first 6 should be listed followed by 'et al.' For further details you are referred to 'Uniform Requirements for Manuscripts submitted to Biomedical Journals' (J Am Med Assoc 1997;277:927–34) (see also Samples of Formatted References).

Video

Elsevier accepts video material and animation sequences to support and enhance your scientific research. Authors who have video or animation files that they wish to submit with their article are strongly encouraged to include links to these within the body of the article. This can be done in the same way as a figure or table by referring to the video or animation content and noting in the body text where it should be placed. All submitted files should be properly labeled so that they directly relate to the video file's content. In order to ensure that your video or animation material is directly usable, please provide the file in one of our recommended file formats with a preferred maximum size of 150 MB per file, 1 GB in total. Video and animation files supplied will be published online in the electronic version of your article in Elsevier Web products, including ScienceDirect. Please supply 'stills' with your files: you can choose any frame from the video or animation or make a separate image. These will be used instead of standard icons and will personalize the link to your video data. For more detailed instructions please visit our video instruction pages. Note: since video and animation cannot be embedded in the print version of the journal, please provide text for both the electronic and the print version for the portions of the article that refer to this content.

Supplementary material

Supplementary material such as applications, images and sound clips, can be published with your article to enhance it. Submitted supplementary items are published exactly as they are received (Excel or PowerPoint files will appear as such online). Please submit your material together with the article and supply a concise, descriptive caption for each supplementary file. If you wish to make changes to supplementary material during any stage of the process, please make sure to provide an updated file. Do not annotate any corrections on a previous version. Please switch off the 'Track Changes' option in Microsoft Office files as these will appear in the published version.

Research data

This journal encourages and enables you to share data that supports your research publication where appropriate, and enables you to interlink the data with your published articles. Research

data refers to the results of observations or experimentation that validate research findings. To facilitate reproducibility and data reuse, this journal also encourages you to share your software, code, models, algorithms, protocols, methods and other useful materials related to the project.

Below are a number of ways in which you can associate data with your article or make a statement about the availability of your data when submitting your manuscript. If you are sharing data in one of these ways, you are encouraged to cite the data in your manuscript and reference list. Please refer to the "References" section for more information about data citation. For more information on depositing, sharing and using research data and other relevant research materials, visit the research data page.

Data linking

If you have made your research data available in a data repository, you can link your article directly to the dataset. Elsevier collaborates with a number of repositories to link articles on ScienceDirect with relevant repositories, giving readers access to underlying data that gives them a better understanding of the research described.

There are different ways to link your datasets to your article. When available, you can directly link your dataset to your article by providing the relevant information in the submission system. For more information, visit the database linking page.

For supported data repositories a repository banner will automatically appear next to your published article on ScienceDirect.

In addition, you can link to relevant data or entities through identifiers within the text of your manuscript, using the following format: Database: xxxx (e.g., TAIR: AT1G01020; CCDC: 734053; PDB: 1XFN).

Mendeley Data

This journal supports Mendeley Data, enabling you to deposit any research data (including raw and processed data, video, code, software, algorithms, protocols, and methods) associated with your manuscript in a free-to-use, open access repository. During the submission process, after uploading your manuscript, you will have the opportunity to upload your relevant datasets directly to *Mendeley Data*. The datasets will be listed and directly accessible to readers next to your published article online.

For more information, visit the Mendeley Data for journals page.

Data statement

To foster transparency, we encourage you to state the availability of your data in your submission. This may be a requirement of your funding body or institution. If your data is unavailable to access or unsuitable to post, you will have the opportunity to indicate why during the submission process, for example by stating that the research data is confidential. The statement will appear with your published article on ScienceDirect. For more information, visit the Data Statement page.

After Acceptance

Online proof correction

To ensure a fast publication process of the article, we kindly ask authors to provide us with their proof corrections within two days. Corresponding authors will receive an e-mail with a link to our online proofing system, allowing annotation and correction of proofs online. The environment is similar to MS Word: in addition to editing text, you can also comment on figures/tables and answer questions from the Copy Editor. Web-based proofing provides a faster and less error-prone process by allowing you to directly type your corrections, eliminating the potential introduction of errors.
If preferred, you can still choose to annotate and upload your edits on the PDF version. All instructions for proofing will be given in the e-mail we send to authors, including alternative methods to the online version and PDF.
We will do everything possible to get your article published quickly and accurately. Please use this proof only for checking the typesetting, editing, completeness and correctness of the text, tables and figures. Significant changes to the article as accepted for publication will only be considered at this stage with permission from the Editor. It is important to ensure that all corrections are sent back to us in one communication. Please check carefully before replying, as inclusion of any subsequent corrections cannot be guaranteed. Proofreading is solely your responsibility.

Offprints

The corresponding author will, at no cost, receive a customized Share Link providing 50 days free access to the final published version of the article on ScienceDirect. The Share Link can be used for sharing the article via any communication channel, including email and social media. For an extra charge, paper offprints can be ordered via the offprint order form which is sent once the article is accepted for publication. Both corresponding and co-authors may order offprints at any time via Elsevier's Author Services. Corresponding authors who have published their article gold open access do not receive a Share Link as their final published version of the article is available open access on ScienceDirect and can be shared through the article DOI link.

Author Inquiries

Visit the Elsevier Support Center to find the answers you need. Here you will find everything from Frequently Asked Questions to ways to get in touch.
You can also check the status of your submitted article or find out when your accepted article will be published.